

NEURAL COLLAPSE UNDER MSE LOSS: PROXIMITY TO AND DYNAMICS ON THE CENTRAL PATH

X.Y. Han*

Cornell University
xh332@cornell.edu

Vardan Papyan*

University of Toronto
vardan.papyan@utoronto.ca

David L. Donoho

Stanford University
donoho@stanford.edu

ABSTRACT

The recently discovered Neural Collapse (NC) phenomenon occurs pervasively in today’s deep net training paradigm of driving cross-entropy (CE) loss towards zero. During NC, last-layer features collapse to their class-means, both classifiers and class-means collapse to the same Simplex Equiangular Tight Frame, and classifier behavior collapses to the nearest-class-mean decision rule. Recent works demonstrated that deep nets trained with mean squared error (MSE) loss perform comparably to those trained with CE. We empirically establish that NC emerges in such MSE-trained deep nets as well through experiments on three canonical networks and five benchmark datasets. We provide, in a Google Colab notebook, PyTorch code for reproducing MSE-NC and CE-NC: [here](#). The analytically-tractable MSE loss offers more mathematical opportunities than the hard-to-analyze CE loss, inspiring us to leverage MSE loss towards the theoretical investigation of NC. We develop three main contributions: (I) We show a new decomposition of the MSE loss into (A) terms directly interpretable through the lens of NC and which assume the last-layer classifier is exactly the least-squares classifier; and (B) a term capturing the deviation from this least-squares classifier. (II) We exhibit experiments on canonical datasets and networks demonstrating that term-(B) is negligible during training. This motivates us to introduce a new theoretical construct: the *central path*, where the linear classifier stays MSE-optimal for feature activations throughout the dynamics. (III) By studying renormalized gradient flow along the central path, we derive exact dynamics that predict NC.

1 INTRODUCTION

Modern deep net training combines practices that amount to paradigms: Some examples are multi-layered architectures, stochastic gradient descent, batch normalization, cross-entropy (CE) loss, and training past *zero error* towards *zero loss*. Understanding the properties of these practices is an important research task.

1.1 NEURAL COLLAPSE

Papyan, Han, and Donoho (2020) recently exposed a striking **Neural Collapse** (NC) phenomenon that emerges during the training of classification deep nets. NC unfolds during the **Terminal Phase of Training** (TPT) during which training proceeds past *zero error* towards *zero CE loss*. The error is defined by

$$\text{Error} = \text{Ave}_{i,c} \mathbf{1}\{c \neq \arg \max_{c'} \langle \mathbf{w}_{c'}, \mathbf{h}_{i,c} \rangle + b_{c'}\},$$

*Equal contribution. Listed alphabetically.

and the CE loss is defined by

$$\text{CE} = -\text{Ave}_{i,c} \log \frac{\exp\{\langle \mathbf{w}_c, \mathbf{h}_{i,c} \rangle + b_c\}}{\sum_{c'=1}^C \exp\{\langle \mathbf{w}_{c'}, \mathbf{h}_{i,c} \rangle + b_{c'}\}},$$

where Ave is the operator that averages over its subscript indices, $\mathbf{w}_c \in \mathbb{R}^P$ and $b_c \in \mathbb{R}$ are the c -th class classifier and bias, $\mathbf{h}_{i,c} \in \mathbb{R}^P$ are the last-layer features of the i -th training example in the c -th class, and C is the number of classes.

NC is defined relative to the feature global mean,

$$\boldsymbol{\mu}_G = \text{Ave}_{i,c} \mathbf{h}_{i,c},$$

the feature class-means,

$$\boldsymbol{\mu}_c = \text{Ave}_i \mathbf{h}_{i,c}, \quad c = 1, \dots, C,$$

and the feature within-class covariance,

$$\boldsymbol{\Sigma}_W = \text{Ave}_{i,c} (\mathbf{h}_{i,c} - \boldsymbol{\mu}_c)(\mathbf{h}_{i,c} - \boldsymbol{\mu}_c)^\top. \quad (1)$$

When the dataset is balanced i.e. when the number of examples per class, N , is equal for all classes¹, NC is characterized by the following four limiting behaviors where limits take place with increasing training epoch t :

(NC1) Within-class variability collapse:

$$\boldsymbol{\Sigma}_W \rightarrow \mathbf{0}$$

(NC2) Convergence to Simplex ETF:

$$\frac{\langle \boldsymbol{\mu}_c - \boldsymbol{\mu}_G, \boldsymbol{\mu}_{c'} - \boldsymbol{\mu}_G \rangle}{\|\boldsymbol{\mu}_c - \boldsymbol{\mu}_G\|_2 \|\boldsymbol{\mu}_{c'} - \boldsymbol{\mu}_G\|_2} \rightarrow \begin{cases} 1, & c = c' \\ -\frac{1}{C-1}, & c \neq c' \end{cases}$$

$$\|\boldsymbol{\mu}_c - \boldsymbol{\mu}_G\|_2 - \|\boldsymbol{\mu}_{c'} - \boldsymbol{\mu}_G\|_2 \rightarrow 0 \quad \forall c \neq c'$$

(NC3) Convergence to self-duality:

$$\frac{\mathbf{w}_c}{\|\mathbf{w}_c\|_2} - \frac{\boldsymbol{\mu}_c - \boldsymbol{\mu}_G}{\|\boldsymbol{\mu}_c - \boldsymbol{\mu}_G\|_2} \rightarrow \mathbf{0}$$

(NC4): Simplification to nearest class center:

$$\arg \max_{c'} \langle \mathbf{w}_{c'}, \mathbf{h} \rangle + b_{c'} \rightarrow \arg \min_{c'} \|\mathbf{h} - \boldsymbol{\mu}_{c'}\|_2$$

(NC2) captures convergence to a simple geometric structure called an *Equiangular Tight Frame* (ETF). An ETF is a collection of vectors $\{\mathbf{v}_c\}_{c=1}^C$ having equal lengths and equal, maximally separated pair-wise angles. In modern classification deep nets, last-layer features are always of higher dimension than the number of classes i.e. $P > C$. In this setting, the maximal pair-wise angles are given by

$$\frac{\langle \mathbf{v}_c, \mathbf{v}_{c'} \rangle}{\|\mathbf{v}_c\|_2 \|\mathbf{v}_{c'}\|_2} = \begin{cases} 1, & \text{for } c = c' \\ -\frac{1}{C-1}, & \text{for } c \neq c' \end{cases},$$

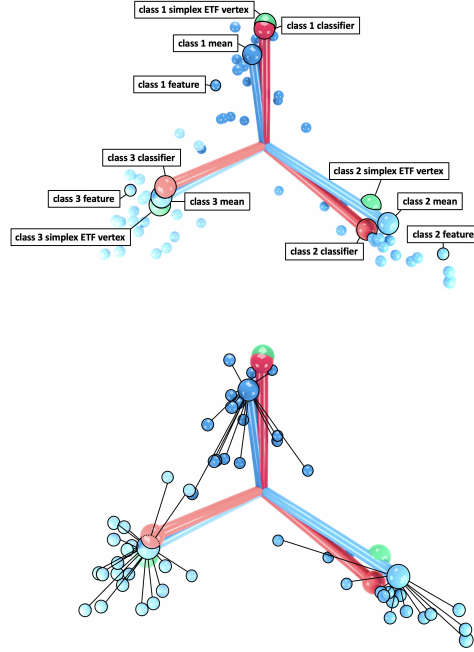


Figure 1: *Portrait of Neural Collapse*. Top figure depicts the last-layer features, class-means, and classifiers with which NC is defined—as well as the Simplex ETF to which they all converge with training. Bottom figure shows the deviations of features from their corresponding class-means. *Reproduced and modified from Figure 1 of Papayan, Han, and Donoho (2020).*

¹Similar to Papayan, Han, and Donoho (2020), we focus on the canonical setting of balanced datasets in this paper. Recent work by Fang et al. (2021) explores NC for imbalanced classes.

and the ETF is called a Simplex ETF². Observe that as C increases, the ETF approaches a (partial) orthogonal matrix. Thus, when C is large, this translates to the intuitive notion that classifiers and class-means tend with training to (near) orthogonality.

1.2 DEEP NET CLASSIFICATION WITH MSE LOSS

While classification deep nets are typically trained with CE loss, Demirkaya et al. (2020) and Hui & Belkin (2020) recently reported deep nets trained with squared error (MSE) loss,

$$\begin{aligned}\mathcal{L}(\mathbf{W}, \mathbf{b}, \mathbf{H}) &= \frac{1}{2} \text{Ave}_{i,c} \|\mathbf{W}\mathbf{h}_{i,c} + \mathbf{b} - \mathbf{y}_{i,c}\|_2^2 + \frac{\lambda}{2} (\|\mathbf{W}\|_F^2 + \|\mathbf{b}\|_2^2) \\ &= \frac{1}{2CN} \|\mathbf{W}\mathbf{H} + \mathbf{b}\mathbf{1}_{CN}^\top - \mathbf{Y}\|_F^2 + \frac{\lambda}{2} (\|\mathbf{W}\|_F^2 + \|\mathbf{b}\|_2^2),\end{aligned}\quad (2)$$

achieve comparable test performance as those trained with CE loss. Above, $\mathbf{H} \in \mathbb{R}^{P \times CN}$ and $\mathbf{Y} \in \mathbb{R}^{C \times CN}$ are matrices resulting from stacking³ together the feature vectors $\mathbf{h}_{i,c}$ and one-hot vectors $\mathbf{y}_{i,c}$ as their respective columns; $\mathbf{W} \in \mathbb{R}^{C \times P}$ is the matrix resulting from the stacking of classifiers \mathbf{w}_c as rows; $\mathbf{b} \in \mathbb{R}^C$ is the vector resulting from concatenating the scalars $\{b_c\}_{c=1}^C$; and $\mathbf{1}_{CN}$ is the length- CN vector of ones. The analytically-tractable MSE loss offers more mathematical opportunities than the hard-to-analyze CE loss and inspires this paper’s main theoretical contributions explicitly characterizing MSE-NC.

1.3 CONTRIBUTIONS

As a preliminary, we *complement* this paper with new, extensive measurements on five benchmark datasets (MNIST, FashionMNIST, SVHN, CIFAR10, and STL10)⁴ and three canonical deep nets (VGG, ResNet, and DenseNet) that verify the empirical reality of MSE-NC i.e. they show **(NC1)**-**(NC4)** indeed occur for networks trained with MSE loss. These experiments are *auxiliary* deliverables establishing that mathematical modeling and analysis of MSE-NC is empirically well-motivated. But, they are lengthy—together spanning four pages with seven figures and a table. Since this paper is mainly a theoretical, we collectively defer these NC-verification experiments to Appendix A.

Having motivated the MSE perspective, Theorem 1 in Section 2 decomposes the MSE loss (Equation 2) into two components:

$$\mathcal{L}(\mathbf{W}, \mathbf{b}, \mathbf{H}) = \mathcal{L}_{\text{LS}}(\mathbf{H}) + \mathcal{L}_{\text{LS}}^\perp(\mathbf{W}, \mathbf{b}, \mathbf{H}), \quad (3)$$

where

$$\mathcal{L}_{\text{LS}}(\mathbf{H}) = \frac{1}{2} \text{Ave}_{i,c} \|\mathbf{W}_{\text{LS}}\mathbf{h}_{i,c} + \mathbf{b}_{\text{LS}} - \mathbf{y}_{i,c}\|_2^2 + \frac{\lambda}{2} (\|\mathbf{W}_{\text{LS}}\|_F^2 + \|\mathbf{b}_{\text{LS}}\|_2^2).$$

Above, \mathbf{W}_{LS} and \mathbf{b}_{LS} are the least-squares (LS) solutions to Equation 2 for some given \mathbf{H} . Note that $\mathcal{L}_{\text{LS}}(\mathbf{H})$ is simply the MSE-loss performance of the optimal $(\mathbf{W}_{\text{LS}}(\mathbf{H}), \mathbf{b}_{\text{LS}}(\mathbf{H}))$ pair on their corresponding \mathbf{H} —where the $\mathbf{W}_{\text{LS}}(\cdot), \mathbf{b}_{\text{LS}}(\cdot)$ notation emphasizes that \mathbf{W}_{LS} and \mathbf{b}_{LS} are *functions* of the given features. Theorem 2 in Section 2 further identifies an NC-interpretable decomposition of \mathcal{L}_{LS} :

$$\mathcal{L}_{\text{LS}}(\mathbf{H}) = \mathcal{L}_{\text{NC1}}(\mathbf{H}) + \mathcal{L}_{\text{NC2/3}}(\mathbf{H}).$$

As will be elaborated upon in Section 2, convergence of \mathcal{L}_{NC1} to zero implies **(NC1)**, while convergence of $\mathcal{L}_{\text{NC2/3}}$ to zero implies **(NC2)** and **(NC3)**. The remaining $\mathcal{L}_{\text{LS}}^\perp(\mathbf{W}, \mathbf{b}, \mathbf{H})$ term (given explicitly later in Theorem 1) measures the deviation of (\mathbf{W}, \mathbf{b}) from $(\mathbf{W}_{\text{LS}}, \mathbf{b}_{\text{LS}})$.

²Traditional research on ETFs (cf. Strohmer & Heath Jr (2003); Fickus & Mixon (2015)) examines the $P \leq C$ setting where C ETF-vectors span their ambient \mathbb{R}^P space. However, in the $P > C$ setting of classification deep nets, the vectors can not span \mathbb{R}^P . Following the precedent of Pappas, Han, and Donoho (2020), we interpret ETFs as equal-length and maximally-equiangular vectors that are not necessarily spanning.

³Assume the stacking is performed in *i-then-c order*: the first column is $(i, c) = (1, 1)$, the second is $(i, c) = (2, 1), \dots$, the N -th is $(i, c) = (N, 1)$, the $(N + 1)$ -st is $(i, c) = (1, 2)$, and so on. This matters for formalizing Equation 12 in Corollary 2.

⁴CIFAR100 and ImageNet are omitted because Demirkaya et al. (2020); Hui & Belkin (2020) showed that they require an additional scaling-heuristic on top of the traditional MSE loss. Rigorous investigation into this scaling-heuristic would have demanded mathematical analysis *outside the scope* of this paper as well as experimentation that would have consumed *expensive* amounts of computational resources.

Figure 2 in Section 2 measures the terms of the above decomposition on the aforementioned canonical dataset-network combinations. It shows that $\mathcal{L}_{\text{LS}}^\perp(\mathbf{W}, \mathbf{b}, \mathbf{H})$ becomes negligible compared to $\mathcal{L}_{\text{LS}}(\mathbf{H})$ when training canonical deep nets on benchmark datasets. In other words, $\mathcal{L}(\mathbf{W}, \mathbf{b}, \mathbf{H}) \approx \mathcal{L}_{\text{LS}}(\mathbf{H})$ occurs early in training and persists into TPT. This motivates us to formulate and analyze a new theoretical construct in Section 3: the *central path*. The central path is the collection of classifier-bias-feature tuples where the classifier and bias are least-squares optimal relative to the given feature:

$$\mathcal{P} = \{(\mathbf{W}_{\text{LS}}(\mathbf{H}), \mathbf{b}_{\text{LS}}(\mathbf{H}), \mathbf{H}) \mid \mathbf{H} \in \mathbb{R}^{P \times CN}\}. \quad (4)$$

In particular, for tuples $(\mathbf{W}, \mathbf{b}, \mathbf{H}) \in \mathcal{P}$, the loss satisfies $\mathcal{L}(\mathbf{W}, \mathbf{b}, \mathbf{H}) = \mathcal{L}_{\text{LS}}(\mathbf{H})$.

The central path shifts focus from \mathcal{L} to \mathcal{L}_{LS} . The loss \mathcal{L}_{LS} satisfies the *invariance property* that $\mathcal{L}_{\text{LS}}(\mathbf{H}) = \mathcal{L}_{\text{LS}}(\mathbf{A}\mathbf{H})$ for any invertible matrix \mathbf{A} , as will be shown in Section 3. Mathematically, the invariance induces an equivalence-class of *equally-performing features*. We choose the *representer* of the equivalence class of \mathbf{H} to be the *renormalized features* $\mathbf{X} = \Sigma_{\mathbf{W}}^{-\frac{1}{2}} \mathbf{H}$ (corresponding to $\mathbf{A} = \Sigma_{\mathbf{W}}^{-\frac{1}{2}}$), whose within-class covariance is the identity matrix. Within the *unconstrained features* (Mixon et al., 2020) or *layer-peeled* (Fang et al., 2021) framework⁵, the dynamics of \mathbf{X} on the central path follow

$$\frac{d}{dt} \mathbf{X} = -\Pi_{T_{\mathbf{X}} \mathcal{X}} (\nabla_{\mathbf{X}} \mathcal{L}_{\text{LS}}(\mathbf{X})), \quad (5)$$

where the operator $\Pi_{T_{\mathbf{X}} \mathcal{X}}$ projects the gradient onto the manifold, \mathcal{X} , of all identity-covariance features. Intuitively, the above constitutes a gradient flow where we continually “renormalize” features to their equivalently-performing representer. Thus, we call Equation 5 the *continually renormalized gradient flow*. We not only show that this flow implies (NC1)-(NC4), but also derive closed-form solutions of the dynamics. The solutions are *explicit* in terms of the singular values and the singular vectors of the renormalized feature class-means at *initialization*.

To summarize, our contributions are as follows:

- We propose a new *decomposition of the MSE loss*: $\mathcal{L} = \mathcal{L}_{\text{NC1}} + \mathcal{L}_{\text{NC2/3}} + \mathcal{L}_{\text{LS}}^\perp$. The terms \mathcal{L}_{NC1} and $\mathcal{L}_{\text{NC2/3}}$ possess interpretations attributable to NC phenomena and assume the classifier \mathbf{W} is exactly the least-squares classifier \mathbf{W}_{LS} ; and $\mathcal{L}_{\text{LS}}^\perp$ captures the deviation of \mathbf{W} from \mathbf{W}_{LS} . (Section 2)
- We introduce a new theoretical construct, the *central path*, where $\mathcal{L}_{\text{LS}}^\perp = 0$. It is inspired by empirical measurements of our decomposition (Figure 2) on realistic dataset-network combinations showing that $\mathcal{L}_{\text{LS}}^\perp$ becomes negligible during training. (Section 3)
- We reveal a key *invariance property* on the central path. The invariance motivates the examination of a representative set of features, $\mathbf{X} = \Sigma_{\mathbf{W}}^{-\frac{1}{2}} \mathbf{H}$, that we call *renormalized features*. (Sections 3.1-3.2)
- We study the gradient flow of those renormalized features along the central path (Equation 5) and derive *exact, closed-form dynamics* that imply NC. The dynamics are explicit in terms of the *singular value decomposition* of the *renormalized feature class-means* at initialization. (Section 3.3)
- We supplement this paper with extensive experiments on five benchmark datasets and three canonical networks that verify *NC phenomena indeed occur on deep nets trained with MSE loss*. (Appendix A)

2 DECOMPOSITION OF MSE LOSS

Inspired by the community’s interest in the role of the MSE loss in deep net training (Demirkaya et al., 2020; Hui & Belkin, 2020; Mixon et al., 2020; Poggio & Liao, 2020a;b), we derive a new

⁵Both the unconstrained features model (Mixon et al., 2020) and the (1-)layer-peeled model (Fang et al., 2021) advocate for the mathematical analysis of deep nets through variants of gradient flow directly on the last-layer features and classifiers. The layer-peeled model is so-named because it proposes to analyze deep nets by “peeling away” one layer at a time. The unconstrained features model is so-named because features are not constrained to be the output of a deep net forward pass but are rather free variables that can be optimized directly: This captures the nearly unlimited flexibility afforded to feature engineering transformations in modern deep nets by the many nonlinear, overparameterized layers.

decomposition of the MSE loss that gives insights into the NC phenomenon. First, absorb the bias vector into the weight matrix—by defining the extended weight matrix $\widetilde{\mathbf{W}} = [\mathbf{W}, \mathbf{b}] \in \mathbb{R}^{C \times (P+1)}$ and the extended feature vector $\widetilde{\mathbf{h}}_{i,c} = [\mathbf{h}_{i,c}; 1] \in \mathbb{R}^{P+1}$ —so that Equation 2 can be rewritten as

$$\mathcal{L}(\widetilde{\mathbf{W}}, \widetilde{\mathbf{H}}) = \frac{1}{2} \text{Ave}_{i,c} \|\widetilde{\mathbf{W}} \widetilde{\mathbf{h}}_{i,c} - \mathbf{y}_{i,c}\|_2^2 + \frac{\lambda}{2} \|\widetilde{\mathbf{W}}\|_F^2. \quad (6)$$

Using $\{\widetilde{\mathbf{h}}_{i,c}\}$, define the entities $\widetilde{\boldsymbol{\mu}}_c$, $\widetilde{\boldsymbol{\mu}}_G$, $\widetilde{\mathbf{H}}$, and $\widetilde{\boldsymbol{\Sigma}}_W$ analogously to those in Section 1.1. We further define the extended total covariance and extended class-means matrices, respectively, as

$$\begin{aligned} \widetilde{\boldsymbol{\Sigma}}_T &= \text{Ave}_{i,c} (\widetilde{\mathbf{h}}_{i,c} - \widetilde{\boldsymbol{\mu}}_G)(\widetilde{\mathbf{h}}_{i,c} - \widetilde{\boldsymbol{\mu}}_G)^\top \in \mathbb{R}^{(P+1) \times (P+1)} \\ \widetilde{\mathbf{M}} &= [\widetilde{\boldsymbol{\mu}}_1, \dots, \widetilde{\boldsymbol{\mu}}_C] \in \mathbb{R}^{(P+1) \times C}. \end{aligned}$$

Next, we reformulate, with weight decay incorporated, a classic result of Webb & Lowe (1990):

Proposition 1 (Webb & Lowe (1990) with Weight Decay). *For fixed extended features $\widetilde{\mathbf{H}}$, the optimal classifier minimizing the MSE loss $\mathcal{L}(\widetilde{\mathbf{W}}, \widetilde{\mathbf{H}})$ is*

$$\widetilde{\mathbf{W}}_{LS} = \frac{1}{C} \widetilde{\mathbf{M}}^\top (\widetilde{\boldsymbol{\Sigma}}_T + \lambda \mathbf{I})^{-1},$$

where \mathbf{I} is the identity matrix. Note that $\widetilde{\mathbf{W}}_{LS}$ depends on $\widetilde{\mathbf{H}}$ only.

Based on $\widetilde{\mathbf{W}}_{LS}$, we identify a new decomposition of the MSE loss:

Theorem 1. (Decomposition of MSE Loss; Proof in Appendix B) *The MSE loss, $\mathcal{L}(\widetilde{\mathbf{W}}, \widetilde{\mathbf{H}})$, can be decomposed into two terms, $\mathcal{L}(\widetilde{\mathbf{W}}, \widetilde{\mathbf{H}}) = \mathcal{L}_{LS}(\widetilde{\mathbf{H}}) + \mathcal{L}_{LS}^\perp(\widetilde{\mathbf{W}}, \widetilde{\mathbf{H}})$, where*

$$\mathcal{L}_{LS}(\widetilde{\mathbf{H}}) = \frac{1}{2} \text{Ave}_{i,c} \|\widetilde{\mathbf{W}}_{LS} \widetilde{\mathbf{h}}_{i,c} - \mathbf{y}_{i,c}\|_2^2 + \frac{\lambda}{2} \|\widetilde{\mathbf{W}}_{LS}\|_F^2,$$

and

$$\mathcal{L}_{LS}^\perp(\widetilde{\mathbf{W}}, \widetilde{\mathbf{H}}) = \frac{1}{2} \text{tr} \left\{ (\widetilde{\mathbf{W}} - \widetilde{\mathbf{W}}_{LS}) \left(\widetilde{\boldsymbol{\Sigma}}_T + \widetilde{\boldsymbol{\mu}}_G \widetilde{\boldsymbol{\mu}}_G^\top + \lambda \mathbf{I} \right) (\widetilde{\mathbf{W}} - \widetilde{\mathbf{W}}_{LS})^\top \right\}.$$

The \mathcal{L}_{LS} component measures the performance of the least-squares classifier $\widetilde{\mathbf{W}}_{LS}$ on $\widetilde{\mathbf{H}}$ i.e. the MSE loss of $\widetilde{\mathbf{H}}$ on the central path (Equation 4). The component $\mathcal{L}_{LS}^\perp(\widetilde{\mathbf{W}}, \widetilde{\mathbf{H}})$ is non-negative⁶ and is zero only when $\widetilde{\mathbf{W}} = \widetilde{\mathbf{W}}_{LS}$. Therefore, $\mathcal{L}_{LS}^\perp(\widetilde{\mathbf{H}})$ quantifies the distance of $\widetilde{\mathbf{W}}$ from $\widetilde{\mathbf{W}}_{LS}$. In short, the central path component, $\mathcal{L}_{LS}(\widetilde{\mathbf{H}})$, captures the behavior of the network when the classifier possesses optimal, least squares behavior. Meanwhile, the deviation component, $\mathcal{L}_{LS}^\perp(\widetilde{\mathbf{W}}, \widetilde{\mathbf{H}})$, captures the divergence from that behavior.

We can further decompose $\mathcal{L}_{LS}(\widetilde{\mathbf{H}})$ into two terms, one capturing activation collapse (NC1) and the other capturing convergence to Simplex ETF of both features and classifiers ((NC2) and (NC3)).

Theorem 2. (Decomposition of Central Path Component; Proof in Appendix C) *The central path component, $\mathcal{L}_{LS}(\widetilde{\mathbf{H}})$, of the MSE decomposition in Theorem 1 can be further decomposed into $\mathcal{L}_{LS}(\widetilde{\mathbf{H}}) = \mathcal{L}_{NC1}(\widetilde{\mathbf{H}}) + \mathcal{L}_{NC2/3}(\widetilde{\mathbf{H}})$, where*

$$\mathcal{L}_{NC1}(\widetilde{\mathbf{H}}) = \frac{1}{2} \text{tr} \left\{ \widetilde{\mathbf{W}}_{LS} \left(\widetilde{\boldsymbol{\Sigma}}_W + \lambda \mathbf{I} \right) \widetilde{\mathbf{W}}_{LS}^\top \right\},$$

and

$$\mathcal{L}_{NC2/3}(\widetilde{\mathbf{H}}) = \frac{1}{2C} \|\widetilde{\mathbf{W}}_{LS} \widetilde{\mathbf{M}} - \mathbf{I}\|_F^2.$$

Inspection of these terms is revealing. For example, \mathcal{L}_{NC1} is characterized by its within-class covariance term—implying that it measures the deviations of last-layer features from class-means. As \mathcal{L}_{NC1} decreases, individual activations would need to tend to their corresponding class-means. Similarly, the approach of the $\widetilde{\mathbf{W}}_{LS} \widetilde{\mathbf{M}}$ term in $\mathcal{L}_{NC2/3}$ towards identity can be directly attributed to the onset of (NC2) and (NC3)⁷. Figure 2 measures the empirical values of the above decomposition terms on five canonical datasets and three prototypical networks.

⁶The middle term is the sum of positive-semidefinite matrices—one of which is positive-definite.

⁷Appendices C.1-C.2 provides additional intuitions on the decomposition terms.

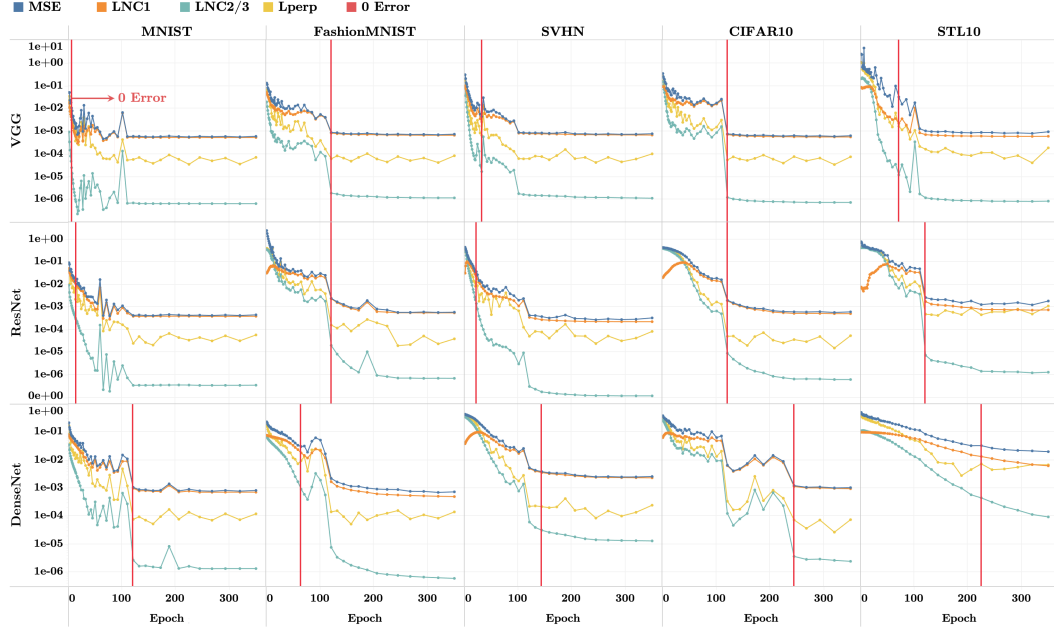


Figure 2: *Decomposition of MSE loss*: Each array column shows a benchmark image classification dataset while each row shows a canonical deep net architecture trained with MSE loss. The red vertical line indicates the epoch at which zero training error was achieved. In each array cell, we plot terms of the MSE loss decomposition $\mathcal{L}(\tilde{\mathbf{W}}, \tilde{\mathbf{H}}) = \mathcal{L}_{\text{NC1}}(\tilde{\mathbf{H}}) + \mathcal{L}_{\text{NC2/3}}(\tilde{\mathbf{H}}) + \mathcal{L}_{\text{LS}}^\perp(\tilde{\mathbf{W}}, \tilde{\mathbf{H}})$ from Section 2. Early in the training, $\mathcal{L}_{\text{LS}}^\perp(\tilde{\mathbf{W}}, \tilde{\mathbf{H}})$ becomes negligible compared to the dominant term, $\mathcal{L}_{\text{NC1}}(\tilde{\mathbf{H}})$, implying $\mathcal{L}_{\text{LS}}^\perp(\tilde{\mathbf{W}}, \tilde{\mathbf{H}}) \ll \mathcal{L}_{\text{LS}}(\tilde{\mathbf{H}}) = \mathcal{L}_{\text{NC1}}(\tilde{\mathbf{H}}) + \mathcal{L}_{\text{NC2/3}}(\tilde{\mathbf{H}})$, i.e. the features and classifiers are *effectively on the central path* during TPT. Further experimental details are in Appendix A. Outlier behavior is discussed in Appendix A.7.

3 EXACT CLOSED-FORM ANALYSIS ON CENTRAL PATH

Consider $\lambda = 0$ in this section. We now state our main theorem:

Theorem 3. (NC Under Continually Renormalized Gradient Flow) *Consider the continually renormalized gradient flow (Equation 5) in which the dynamics are restricted to the central path, and the features are renormalized to identity within-class covariance. Assume the features are initialized with zero global mean. Then, Neural Collapse emerges on the renormalized features with explicit dynamics of the flow given in Proposition 2 as well as Corollaries 1 and 2 later in this paper.*

Three assumptions stand out, which we discuss below:

(A1) Restriction to central path: Figure 2 shows that—in practice, during TPT— $\mathcal{L}_{\text{LS}}^\perp(\tilde{\mathbf{W}}, \tilde{\mathbf{H}})$ is observed to be negligible compared to the dominant term, $\mathcal{L}_{\text{LS}}(\tilde{\mathbf{H}})$. This indicates $(\tilde{\mathbf{W}}, \tilde{\mathbf{H}})$ is close to the central path (Equation 4) where $\mathcal{L}(\tilde{\mathbf{W}}, \tilde{\mathbf{H}}) = \mathcal{L}_{\text{LS}}(\tilde{\mathbf{H}})$.

(A2) Zero global mean: Proximity to the central path implies that the last-layer biases become close to \mathbf{b}_{LS} . Having biases $\mathbf{b} = \mathbf{b}_{\text{LS}}$ is effectively performing classification with no bias term (i.e. using only a linear classifier \mathbf{W}) on *zero-mean data*. To see this, define the globally-centered features, globally-centered means, and total-covariance matrix in unextended coordinates:

$$\bar{\mathbf{H}} = \mathbf{H} - \mu_G \mathbb{1}_{CN}^\top; \quad \bar{\mathbf{M}} = [\mu_1 - \mu_G, \dots, \mu_C - \mu_G]; \quad \Sigma_T = \frac{1}{CN} \bar{\mathbf{H}} \bar{\mathbf{H}}^\top.$$

Proposition 1 then reduces to the following forms for the unextended weights and biases:

$$\tilde{\mathbf{W}}_{\text{LS}} = [\mathbf{W}_{\text{LS}}, \mathbf{b}_{\text{LS}}] = [C^{-1} \bar{\mathbf{M}}^\top \Sigma_T^{-1}, \quad C^{-1} \mathbb{1}_C - C^{-1} \bar{\mathbf{M}}^\top \Sigma_T^{-1} \mu_G]. \quad (7)$$

For an arbitrary activation-target pair (\mathbf{h}, \mathbf{y}) , the prediction error obeys

$$\begin{aligned} \mathbf{W}_{\text{LS}}\mathbf{h} + \mathbf{b}_{\text{LS}} - \mathbf{y} &= C^{-1}\bar{\mathbf{M}}^\top \Sigma_T^{-1}\mathbf{h} + C^{-1}\mathbf{1}_C - C^{-1}\bar{\mathbf{M}}^\top \Sigma_T^{-1}\boldsymbol{\mu}_G - \mathbf{y} \\ &= \mathbf{W}_{\text{LS}}(\mathbf{h} - \boldsymbol{\mu}_G) - (\mathbf{y} - C^{-1}\mathbf{1}_C). \end{aligned}$$

The last line exhibits two terms in parentheses, both traceable to the action of the bias \mathbf{b}_{LS} . The term $\mathbf{h} - \boldsymbol{\mu}_G$ demonstrates that the bias induces a global-mean subtraction on \mathbf{h} , while the term $\mathbf{y} - C^{-1}\mathbf{1}_C$ demonstrates that the bias also induces a global-mean subtraction on the one-hot targets.

(A3) Renormalization to identity covariance: Renormalization is ubiquitous in the empirical deep learning literature through works such batch normalization and its variants (Ioffe & Szegedy, 2015; Salimans & Kingma, 2016; Wu & He, 2018; Ulyanov et al., 2016; Ba et al., 2016; Krizhevsky et al., 2012). It is also ideologically preceded in the theoretical ML literature through works such as Douglas et al. (1998); Banburski et al. (2019); Poggio & Liao (2020a;b). Within this paper, the covariance-renormalization is inspired by an invariance property of the loss as well as the intuitive concept of the signal-to-noise ratio from mathematical statistics (discussed later in Sections 3.1-3.2).

In the subsequent sections, we motivate and introduce the theoretical constructs necessary for proving Theorem 3 and for presenting the explicit dynamics of the flow.

3.1 INVARIANCE PROPERTY

By Assumption (A2), classification on the central path is equivalent to classification on globally-centered features using only the linear classifier \mathbf{W}_{LS} . Then, using Equation 7, we can equivalently represent the central path (Equation 4) as follows:

Definition 1 (Zero Global Mean Central Path).

$$\bar{\mathcal{P}} = \left\{ (\mathbf{W}_{\text{LS}}, \bar{\mathbf{H}}) \mid \mathbf{W}_{\text{LS}} = C^{-1}\bar{\mathbf{M}}^\top \Sigma_T^{-1} \right\}.$$

An *invariance property* holds on the central path: Let \mathbf{A} denote a symmetric, full-rank matrix. Then,

$$\mathbf{W}_{\text{LS}}(\mathbf{A}\bar{\mathbf{H}})\mathbf{A}\bar{\mathbf{H}} = \mathbf{W}_{\text{LS}}(\bar{\mathbf{H}})\mathbf{A}^{-1}\mathbf{A}\bar{\mathbf{H}} = \mathbf{W}_{\text{LS}}(\bar{\mathbf{H}})\bar{\mathbf{H}}, \quad (8)$$

where the notation $\mathbf{W}_{\text{LS}}(\cdot)$ makes explicit that \mathbf{W}_{LS} is a *function* of a set of input features. In other words, the actual predictions made by the least squares classifier are invariant to choice of the coordinates in which we express $\bar{\mathbf{H}}$, i.e. all features $\mathbf{A}\bar{\mathbf{H}}$ are *equivalently performing*. Among those coordinate systems, we will prefer the one in which the “noise” is “whitened” or “sphered.”

Suppose that $\Sigma_W(\bar{\mathbf{H}})$ —where the notation $\Sigma_W(\cdot)$ expresses the within-class covariance as a function features—is positive-definite⁸. Consider the coordinate transformation $\bar{\mathbf{H}} \mapsto \mathbf{A}\bar{\mathbf{H}}$ with $\mathbf{A} = \Sigma_W^{-\frac{1}{2}}(\bar{\mathbf{H}})$. In these coordinates, the features are “renormalized” to spherical covariance,

$$\Sigma_W(\mathbf{A}\bar{\mathbf{H}}) = \mathbf{A}\Sigma_W(\bar{\mathbf{H}})\mathbf{A} = \mathbf{I},$$

so we will call $\mathbf{A}\bar{\mathbf{H}}$ the *renormalized features*. The class-means of $\mathbf{A}\bar{\mathbf{H}}$ are

$$\bar{\mathbf{M}}(\mathbf{A}\bar{\mathbf{H}}) = \mathbf{A}\bar{\mathbf{M}}(\bar{\mathbf{H}}) = \Sigma_W^{-\frac{1}{2}}(\bar{\mathbf{H}})\bar{\mathbf{M}}(\bar{\mathbf{H}}),$$

where the notation $\bar{\mathbf{M}}(\cdot)$ expresses that the means are a function of features. The $\Sigma_W^{-\frac{1}{2}}\bar{\mathbf{M}}$ term evokes the canonical idea of a signal-to-noise ratio from statistics—motivating the next subsection.

3.2 SIGNAL-TO-NOISE RATIO MATRIX ON THE CENTRAL PATH

The classifier in Equation 7 can be rewritten as

$$\mathbf{W}_{\text{LS}} = C^{-1}\bar{\mathbf{M}}^\top (C^{-1}\bar{\mathbf{M}}\bar{\mathbf{M}}^\top + \Sigma_W)^{-1}.$$

⁸Given the definition in Equation 1, the positive-definiteness of Σ_W is unsurprising in deep net contexts because $CN \gg P$ i.e. the number of examples is larger than the width of the last-layer. Moreover, positive-definiteness does not contradict (NC1). (NC1) is characterized by Σ_W *approaching* the zero-matrix with training. The zero-matrix is never actually achieved during the training dynamics, so Σ_W remains full-rank.

The combined presence of the terms $\bar{\mathbf{M}}\bar{\mathbf{M}}^\top$ and Σ_W in the denominator, along with $\bar{\mathbf{M}}$ in the numerator, signals to us the presence of the informative *signal-to-noise (SNR) ratio matrix*:

$$\text{SNR} \equiv \Sigma_W^{-\frac{1}{2}} \bar{\mathbf{M}}. \quad (9)$$

Why this terminology? The globally-centered class-means represent the overall “signal” indicating that the class-means are separated from each other: if they were non-separated—e.g. all equal— $\bar{\mathbf{M}}$ would be zero. However, a classifier decision must keep in view noise—captured by Σ_W —which might confuse the classifier. So, one wishes the signal be large compared to the noise. It may help to consider the mental model—which is not at all necessary to the correctness of our analysis—under which the activations are normally distributed with $\mathbf{h}_{i,c} \sim \mathcal{N}(\boldsymbol{\mu}_c, \Sigma_W)$. Under that model, a linear classifier will indeed get confused if the norm $\|\boldsymbol{\mu}_c - \boldsymbol{\mu}_G\|_2$ is “small compared” to Σ_W . Replacing this somewhat vague statement by a discussion of quantitative properties of the SNR matrix is well understood by mathematical statisticians to be decisive for understanding classification performance in the normal case. Additionally, observe that $\text{SNR} = \bar{\mathbf{M}}(\Sigma_W^{-\frac{1}{2}} \bar{\mathbf{H}})$. Thus, connecting back to Section 3.1, *the SNR matrix is simply the class-means matrix of the renormalized features*.

The SNR can be further understood through its singular value decomposition (SVD).

Definition 2 (SVD of SNR Matrix). *Denote the SVD of the SNR matrix (Equation 9) as follows:*

$$\text{SNR} = \mathbf{U}\mathbf{\Omega}\mathbf{V}^\top = \sum_{j=1}^{C-1} \omega_j \mathbf{u}_j \mathbf{v}_j^\top.$$

Here, $\{\omega_c\}_{c=1}^{C-1}$ are the non-zero singular values of SNR; $\mathbf{\Omega} = \text{diag}(\{\omega_c\}_{c=1}^{C-1}, 0) \in \mathbb{R}^{C \times C}$; and the left and right singular-vectors, $\mathbf{U} \in \mathbb{R}^{P \times C}$ and $\mathbf{V} \in \mathbb{R}^{C \times C}$, are partial orthogonal and orthogonal matrices, respectively, with columns $\{\mathbf{u}_j\}_{j=1}^C$ and $\{\mathbf{v}_j\}_{j=1}^C$. The SNR matrix is rank $C - 1$ since Σ_W is assumed full-rank and $\bar{\mathbf{M}}$ is rank $C - 1$ due to global-mean subtraction.

The non-zero singular values, $\{\omega_j\}_{j=1}^{C-1}$, are decisive for understanding the separation performance of the least-squares linear classifier⁹. As we will see in the next section, examining the dynamics of these singular-values when the features undergo gradient flow in renormalized coordinates lead to precise characterizations of Neural Collapse¹⁰.

3.3 DYNAMICS OF SNR

For any matrix \mathbf{Z} , we use \mathbf{Z}_t in this section to denote the state of that matrix at time t . Similarly, we denote with $\{\omega_j(t)\}_{j=1}^{C-1}$ the state of the non-zero SNR singular values at t . Interpret $t=0$ as the time of training when feature-classifier pairs effectively enter the central path. We now present Proposition 2 and Corollaries 1-2 that provide the explicit dynamics referenced by Theorem 3.

Proposition 2 (Dynamics of Singular Values of SNR Matrix; Proof in Appendix D.4). *Continually renormalized gradient flow on the central path (Equation 5) induces the following closed-form dynamics on the SNR singular values (Definition 2):*

$$c_1 \log(\omega_j(t)) + c_2 \omega_j^2(t) + c_3 \omega_j^4(t) = a_j + t, \quad t \geq 0, \quad \text{for all } j = 1, \dots, C - 1. \quad (10)$$

c_1 , c_2 , and c_3 are positive constants independent of j , and a_j is a constant depending on $\omega_j(0)$.

Corollary 1 (Properties of SNR Singular Values; Proof in Appendix D.5). *SNR singular values (Definition 2) following the Equation 10 dynamics satisfy the following limiting behaviors:*

1. $\lim_{t \rightarrow \infty} \omega_j(t) = \infty$, for all $j = 1, \dots, C - 1$.
2. $\lim_{t \rightarrow \infty} \frac{\omega_j(t)}{\sqrt{\frac{t}{c_4}}} = 1$, for all $j = 1, \dots, C - 1$.

⁹Good performance demands that the singular values be large; indeed the smallest one controls the orthogonal distance of each class-mean from the linear span of the other class-means. Consequently, driving-larger the smallest nonzero singular value makes the task of linear separation more immune to (spherical) noise and to Euclidean-norm-constrained adversarial noise.

¹⁰For additional, supplementary intuitions about invariance, renormalization, and continually renormalized gradient flow, see the exposition in Appendices D.1-D.3.

$$3. \lim_{t \rightarrow \infty} \frac{\max_j \omega_j(t)}{\min_j \omega_j(t)} = 1.$$

Corollary 2 (Neural Collapse under MSE Loss; Proof in Appendix D.6). *The SNR matrix (Equation 9) converges to*

$$\lim_{t \rightarrow \infty} \frac{1}{\omega_{\max}(t)} \text{SNR}_t = \hat{\mathbf{U}}_0 \hat{\mathbf{V}}_0^\top, \quad (11)$$

where $\hat{\mathbf{U}}_0 \in \mathbb{R}^{P \times (C-1)}$ and $\hat{\mathbf{V}}_0 \in \mathbb{R}^{C \times (C-1)}$ are the left and right singular vectors of the SNR matrix (Definition 2) at $t=0$ corresponding to the non-zero singular values; and $\omega_{\max}(t)$ is the largest singular value at time t . Corollary 1 and Equation 11 together imply the occurrence of (NC1)-(NC4) i.e. renormalized gradient flow on the central path leads to Neural Collapse.

Moreover, denoting the Kronecker product with \otimes , the renormalized features matrix converges to

$$\lim_{t \rightarrow \infty} \frac{1}{\omega_{\max}(t)} \Sigma_{W,t}^{-\frac{1}{2}} \bar{\mathbf{H}}_t = (\hat{\mathbf{U}}_0 \hat{\mathbf{V}}_0^\top) \otimes \mathbf{1}_N^\top. \quad (12)$$

4 RELATED WORKS

Since the publication of Pappas, Han, and Donoho (2020), several works (Mixon et al., 2020; Lu & Steinerberger, 2020; E & Wojtowysch, 2020; Poggio & Liao, 2020a;b; Fang et al., 2021; Ergen & Pilanci, 2020; Zhu et al., 2021) proposed mathematical frameworks ratifying Neural Collapse.

Among them, Mixon et al. (2020) and Poggio & Liao (2020a;b) also examine MSE-NC. In particular, Poggio & Liao (2020a;b) examine MSE-NC in homogeneous, weight-normalized networks. Meanwhile, Mixon et al. (2020) studies MSE-NC on networks trained with gradient flow directly on the features-classifier pair—which they name the *unconstrained features model*. This general framework—wherein last-layer features are not constrained to be the output of a deep net forward pass—was concurrently proposed by Fang et al. (2021) (for CE loss) in their *layer-peeled model*.

Our contributions in this paper are *distinct* from the MSE-NC analyses of Mixon et al. (2020) and Poggio & Liao (2020a;b): The work of Mixon et al. (2020) relies on a *linear-approximation* to the unconstrained features model ODE while Poggio & Liao (2020a;b)—in a special section co-authored with Andrzej Banburski—examine *homogeneous, weight-normalized* networks. In contrast, this paper provides a novel NC-intepretable decomposition of the MSE loss. Measurements of this decomposition (Figure 2) then motivate us to introduce the original central path construct on which we analyze renormalized gradient flow. Our derivations result in exact, closed-form dynamics that predict Neural Collapse: Neither Mixon et al. (2020) nor Poggio & Liao (2020a;b) provide exact, closed-form dynamics as we do.

Outside the MSE setting, Lu & Steinerberger (2020); E & Wojtowysch (2020); Ergen & Pilanci (2020); Fang et al. (2021); Zhu et al. (2021) examine the emergence of the NC properties under variants of the unconstrained features/layer-peeled model trained with CE loss. In particular, Lu & Steinerberger (2020) examine the optimization of the classifiers and *class-means*; E & Wojtowysch (2020) examine the optimization of classifiers and features *restricted to the unit ball*; Ergen & Pilanci (2020) and Fang et al. (2021) examine the last-layers of networks that have been reformulated or relaxed to *convex formulations*; and Zhu et al. (2021) examine the properties of the *global minima* of the CE loss with weight decay. These works also do not describe the dynamics and instead focus on characterizing the loss landscape or the global minima.

For more details, we provide a comprehensive survey of all above-mentioned papers in Appendix E.

5 CONCLUSION

In this paper, after verifying that NC occurs when prototypical classification deep nets are trained with MSE loss on canonical datasets, we then derive and measure a novel decomposition of the MSE loss. We observed that the last-layer classifier tends to the least-squares classifier early in training—motivating us to define the central path on which the classifier behaves exactly as optimal least-squares classifier. On the central path, we showed invariance properties that inspired us to examine the renormalized features and their corresponding continually renormalized gradient flow. This flow induces closed-form dynamics that imply the occurrence of Neural Collapse.

REPRODUCIBILITY STATEMENT

This paper is reproducible. Experimental details about all empirical results described in this paper are provided in Appendix A. Additionally, we provide PyTorch (Paszke et al., 2019) code for reproducing NC under both MSE and CE—as well as the Figure 2 MSE decomposition—in the following Google Colaboratory notebook: [here](#). All datasets and networks used in our experiments originate from the PyTorch Model Zoo with pre-processing details described in Appendix A. Formal statements and proofs of all our theoretical results are provided in Appendices B-D.

REFERENCES

- Sanjeev Arora, Simon Du, Wei Hu, Zhiyuan Li, and Ruosong Wang. Fine-grained analysis of optimization and generalization for overparameterized two-layer neural networks. In *International Conference on Machine Learning*, pp. 322–332. PMLR, 2019.
- Jimmy Lei Ba, Jamie Ryan Kiros, and Geoffrey E Hinton. Layer normalization. *arXiv preprint arXiv:1607.06450*, 2016.
- Andrzej Banburski, Qianli Liao, Brando Miranda, Lorenzo Rosasco, Fernanda De La Torre, Jack Hidary, and Tomaso Poggio. Theory iii: Dynamics and generalization in deep networks. *arXiv preprint arXiv:1903.04991*, 2019.
- Andrzej Banburski, Fernanda De La Torre, Nishka Plant, Ishana Shastri, and Tomaso Poggio. Cross-validation stability of deep networks. Technical report, Center for Brains, Minds and Machines (CBMM), 2021.
- Lenaic Chizat and Francis Bach. On the global convergence of gradient descent for over-parameterized models using optimal transport. *Advances in neural information processing systems*, 31:3036–3046, 2018.
- Lenaic Chizat and Francis Bach. Implicit bias of gradient descent for wide two-layer neural networks trained with the logistic loss. *arXiv preprint arXiv:2002.04486*, 2020.
- Ahmet Demirkaya, Jiasi Chen, and Samet Oymak. Exploring the role of loss functions in multiclass classification. In *2020 54th Annual Conference on Information Sciences and Systems (CISS)*, pp. 1–5. IEEE, 2020.
- Scott C Douglas, SY Kung, and Shun-ichi Amari. A self-stabilized minor subspace rule. *IEEE Signal Processing Letters*, 5(12):328–330, 1998.
- Weinan E and Stephan Wojtowytsch. On the emergence of tetrahedral symmetry in the final and penultimate layers of neural network classifiers. *arXiv preprint arXiv:2012.05420*, 2020.
- Tolga Ergen and Mert Pilanci. Revealing the structure of deep neural networks via convex duality. *arXiv preprint arXiv:2002.09773*, 2020.
- Cong Fang, Hangfeng He, Qi Long, and Weijie J Su. Layer-peeled model: Toward understanding well-trained deep neural networks. *arXiv preprint arXiv:2101.12699*, 2021.
- Matthew Fickus and Dustin G Mixon. Tables of the existence of equiangular tight frames. *arXiv preprint arXiv:1504.00253*, 2015.
- Kaiming He, Xiangyu Zhang, Shaoqing Ren, and Jian Sun. Delving deep into rectifiers: Surpassing human-level performance on imagenet classification. In *Proceedings of the IEEE international conference on computer vision*, pp. 1026–1034, 2015.
- Like Hui and Mikhail Belkin. Evaluation of neural architectures trained with square loss vs cross-entropy in classification tasks. *arXiv preprint arXiv:2006.07322*, 2020.
- Sergey Ioffe and Christian Szegedy. Batch normalization: Accelerating deep network training by reducing internal covariate shift. In *International conference on machine learning*, pp. 448–456. PMLR, 2015.

- Alex Krizhevsky, Ilya Sutskever, and Geoffrey E Hinton. Imagenet classification with deep convolutional neural networks. *Advances in neural information processing systems*, 25:1097–1105, 2012.
- Jianfeng Lu and Stefan Steinerberger. Neural collapse with cross-entropy loss. *arXiv preprint arXiv:2012.08465*, 2020.
- Song Mei, Andrea Montanari, and Phan-Minh Nguyen. A mean field view of the landscape of two-layer neural networks. *Proceedings of the National Academy of Sciences*, 115(33):E7665–E7671, 2018.
- Dustin G Mixon, Hans Parshall, and Jianzong Pi. Neural collapse with unconstrained features. *arXiv preprint arXiv:2011.11619*, 2020.
- Vardan Papyan, X. Y. Han, and David L. Donoho. Prevalence of Neural Collapse during the terminal phase of deep learning training. *Proceedings of the National Academy of Sciences*, 117(40):24652–24663, 2020.
- Adam Paszke, Sam Gross, Francisco Massa, Adam Lerer, James Bradbury, Gregory Chanan, Trevor Killeen, Zeming Lin, Natalia Gimelshein, Luca Antiga, et al. Pytorch: An imperative style, high-performance deep learning library. In *Advances in neural information processing systems*, pp. 8026–8037, 2019.
- Tomaso Poggio and Qianli Liao. Explicit regularization and implicit bias in deep network classifiers trained with the square loss. *arXiv preprint arXiv:2101.00072*, 2020a.
- Tomaso Poggio and Qianli Liao. Implicit dynamic regularization in deep networks. Technical report, Center for Brains, Minds and Machines (CBMM), 2020b.
- Grant M Rotskoff and Eric Vanden-Eijnden. Parameters as interacting particles: long time convergence and asymptotic error scaling of neural networks. In *Proceedings of the 32nd International Conference on Neural Information Processing Systems*, pp. 7146–7155, 2018.
- Tim Salimans and Durk P Kingma. Weight normalization: A simple reparameterization to accelerate training of deep neural networks. *Advances in neural information processing systems*, 29:901–909, 2016.
- Thomas Strohmer and Robert W Heath Jr. Grassmannian frames with applications to coding and communication. *Applied and computational harmonic analysis*, 14(3):257–275, 2003.
- James Townsend. Differentiating the singular value decomposition. Technical report, Technical Report 2016, [https://j-towns.github.io/papers/svd-derivative ...](https://j-towns.github.io/papers/svd-derivative...), 2016.
- Dmitry Ulyanov, Andrea Vedaldi, and Victor Lempitsky. Instance normalization: The missing ingredient for fast stylization. *arXiv preprint arXiv:1607.08022*, 2016.
- Andrew R Webb and David Lowe. The optimised internal representation of multilayer classifier networks performs nonlinear discriminant analysis. *Neural Networks*, 3(4):367–375, 1990.
- Yuxin Wu and Kaiming He. Group normalization. In *Proceedings of the European conference on computer vision (ECCV)*, pp. 3–19, 2018.
- Zhihui Zhu, Tianyu Ding, Jinxin Zhou, Xiao Li, Chong You, Jeremias Sulam, and Qing Qu. A geometric analysis of neural collapse with unconstrained features. *arXiv preprint arXiv:2105.02375*, 2021.

APPENDIX

A	MSE Neural Collapse experiments	13
A.1	Datasets	13
A.2	Networks	13
A.3	Optimization methodology	13
A.4	Computational resources	13
A.5	Formatting	14
A.6	Experimental results	14
A.7	Exceptions: STL10-ResNet and STL10-DenseNet	20
A.8	Open Questions: Weight-decay, batch normalization, SGD, generalization, test data	20
B	Theorem 1	21
C	Theorem 2	21
C.1	Intuitions for Theorem 2 in unextended coordinates	22
C.2	Additional intuitions for Theorem 2 terms	22
D	Theorem 3	22
D.1	Implications of invariance	22
D.2	Aligned SNR coordinates	24
D.3	Continually renormalized gradient flow	26
D.4	Proof of Proposition 2 (gradient flow in aligned SNR coordinates)	27
D.5	Proof of Corollary 1	29
D.6	Proof of Corollary 2	30
E	Related works examining Neural Collapse	30
E.1	Mixon, Parshall, and Pi (2020)	30
E.2	Lu and Steinerberger (2020)	31
E.3	E and Wojtowytsch (2020)	31
E.4	Poggio & Liao (2020a;b) (with Banburski)	31
E.5	Ergen & Pilanci (2020)	32
E.6	Fang, He, Long, and Su (2021)	32
E.7	Zhu, Ding, Zhou, Li, You, Sulam, and Qu (2021)	33

A MSE NEURAL COLLAPSE EXPERIMENTS

The experiments in this section examine the properties of Neural Collapse (NC) on deep nets trained using MSE loss. The direct MSE-analogues to the cross-entropy (CE) loss table and figures in Pappan, Han, and Donoho (2020) are in Table 1 and Figures 3-9 here. Furthermore, Figures 10-11 compares the MSE-NC experiments observed in this paper with the CE-NC behaviors in Pappan, Han, and Donoho (2020). Experimental descriptions and discussions are within the captions. Subsections A.1-A.5 describe formatting and experimental details. Then, Subsection A.6 collectively presents all experimental figures for this section. Subsection A.7 addresses outlier behaviors observed in the plots. Finally, Subsection A.8 discusses open questions inspired by NC.

A.1 DATASETS

We consider the MNIST, FashionMNIST, CIFAR10, SVHN, and STL10 datasets with pre-processing the same as in Pappan, Han, and Donoho (2020).

A.1.1 CHOICE OF DATASETS

Demirkaya et al. (2020) and Hui & Belkin (2020) showed multi-class classification deep nets trained with MSE loss—sometimes with a heuristical-scaling—demonstrate comparable test-error performance to those trained with CE loss. Even without additional scaling, i.e. with vanilla MSE loss, we found this true for ten class classification datasets—such as MNIST, FashionMNIST, SVHN, CIFAR10, and STL10—so we focus on these five datasets. For more than ten classes (i.e. datasets such as CIFAR100 and ImageNet), both Demirkaya et al. (2020) and Hui & Belkin (2020) showed that the additional scaling-heuristic does need to be applied to the loss before comparable test-performance can be achieved. In informal, exploratory experiments not reported here, we were able to reproduce their results on datasets with more than ten classes. But, we feel these scaling-heuristics merit further scientific investigation of their own and are beyond the scope of this article¹¹, so we do not include datasets that require scaling-heuristic tuning.

A.2 NETWORKS

We train VGG, ResNet, and DenseNet models with the same depth-selection procedures and architecture-specification choices as in Pappan, Han, and Donoho (2020). In the MSE setting, the final chosen depths were as follows:

DATASET	VGG	RESNET	DENSENET
MNIST	VGG11	RESNET18	DENSENET40
FASHIONMNIST	VGG11	RESNET18	DENSENET250
SVHN	VGG13	RESNET34	DENSENET40
CIFAR10	VGG11	RESNET50	DENSENET100
STL10	VGG11	RESNET18	DENSENET201

A.3 OPTIMIZATION METHODOLOGY

The optimization algorithm, parameters, and hyperparameter tuning are the same as in Pappan, Han, and Donoho (2020).

A.4 COMPUTATIONAL RESOURCES

The experiments were run on our institutional High-Performance Computing (HPC) cluster. Each dataset-network combination was trained on a single GPU attached to a CPU with at least 32GB of RAM—the specific types of the CPUs/GPUs vary according to whichever was first assigned to us by the HPC cluster scheduler.

¹¹Thorough experimentation with this scaling-heuristic would also consume prohibitively expensive amounts of computational resources.

A.5 FORMATTING

The coloring and formatting of the plots are the same as in Pappan, Han, and Donoho (2020).

A.6 EXPERIMENTAL RESULTS

Table 1: Table comparing test-accuracy at moment 0-error is achieved vs. at the end of training. Analogous to Table 1 of Pappan, Han, and Donoho (2020). The median improvement is 0.962 percentage points; the mean is 1.833 percentage points.

DATASET	NET	ACC. 0-ERROR	ACC. FINAL
MNIST	VGG	99.23	99.59
	RESNET	99.16	99.70
	DENSENET	99.62	99.70
FASHION	VGG	92.76	92.95
	RESNET	93.55	93.76
	DENSENET	90.56	92.95
SVHN	VGG	89.35	93.91
	RESNET	85.18	92.65
	DENSENET	95.61	95.23
CIFAR10	VGG	83.13	84.54
	RESNET	75.43	76.39
	DENSENET	91.77	91.78
STL10	VGG	60.43	67.24
	RESNET	59.35	60.56
	DENSENET	58.74	60.41

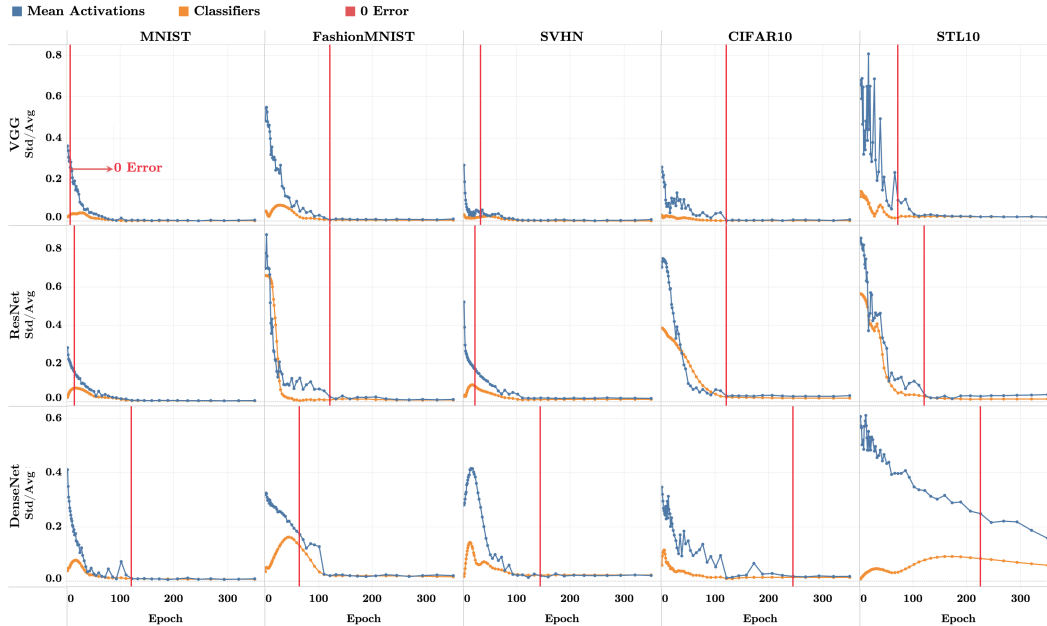


Figure 3: Plots analogous to Figure 2 in Pappan et al. (2020), but on networks trained with MSE Loss. Results demonstrate that last-layer features and classifiers approach *equinormness*.

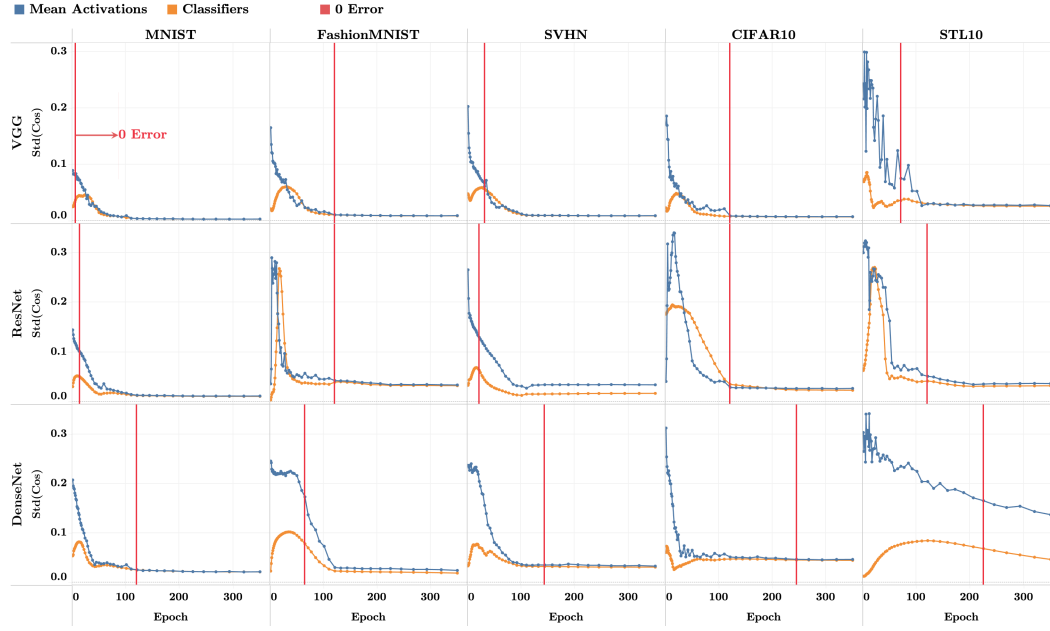


Figure 4: Plots analogous to Figure 3 in Pappan et al. (2020), but on networks trained with MSE Loss. Results demonstrate that last-layer features and classifiers approach *equiangularity*.

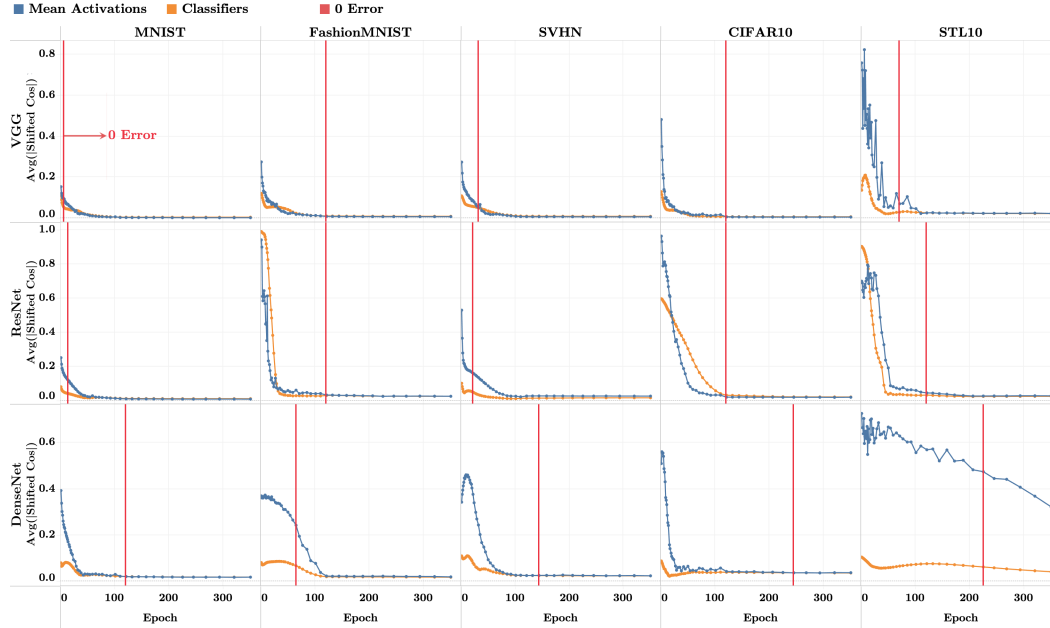


Figure 5: Plots analogous to Figure 4 in Pappan et al. (2020), but on networks trained with MSE Loss. Results demonstrate that last-layer features and classifiers approach *maximal-equiangularity*.

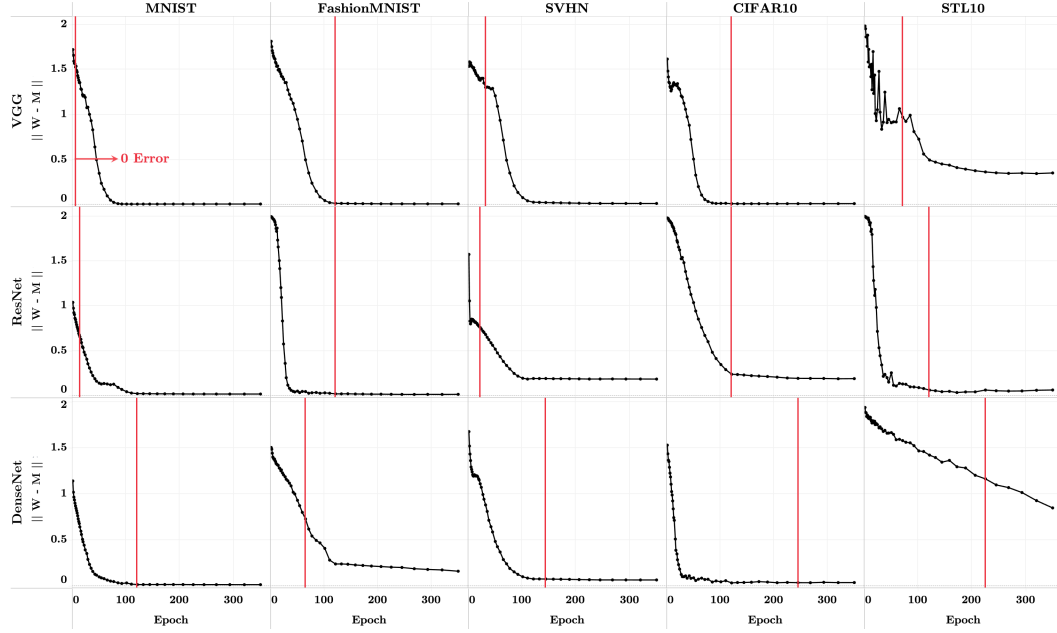


Figure 6: Plots analogous to Figure 5 in Pappan et al. (2020), but on networks trained with MSE Loss. Results demonstrate that last-layer features and classifiers approach *self-duality*.

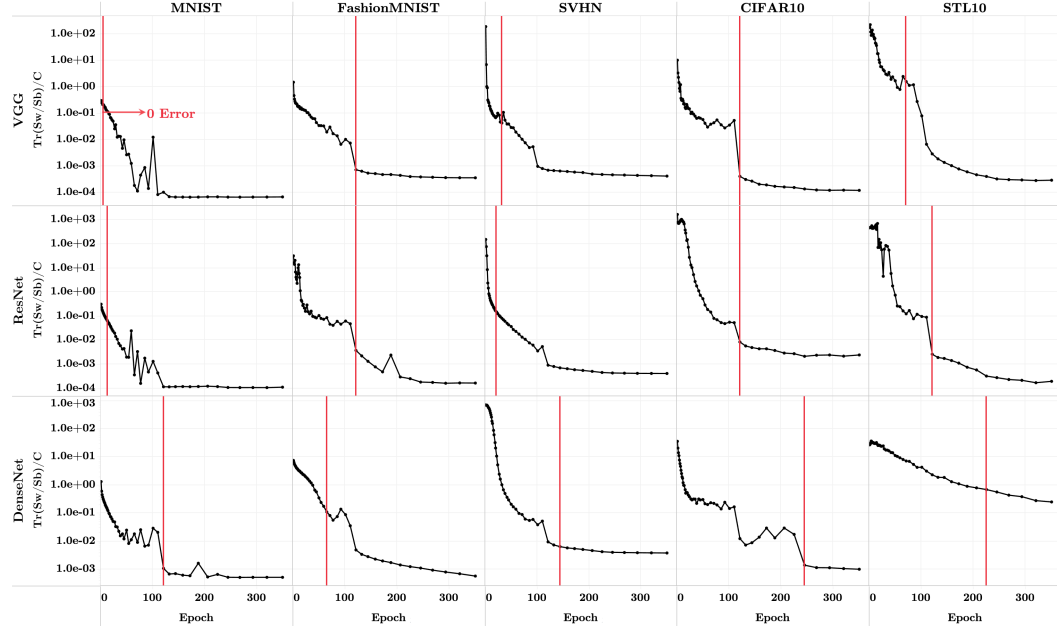


Figure 7: Plots analogous to Figure 6 in Pappan et al. (2020), but on networks trained with MSE Loss. Results demonstrate that last-layer features undergo *variability collapse*.

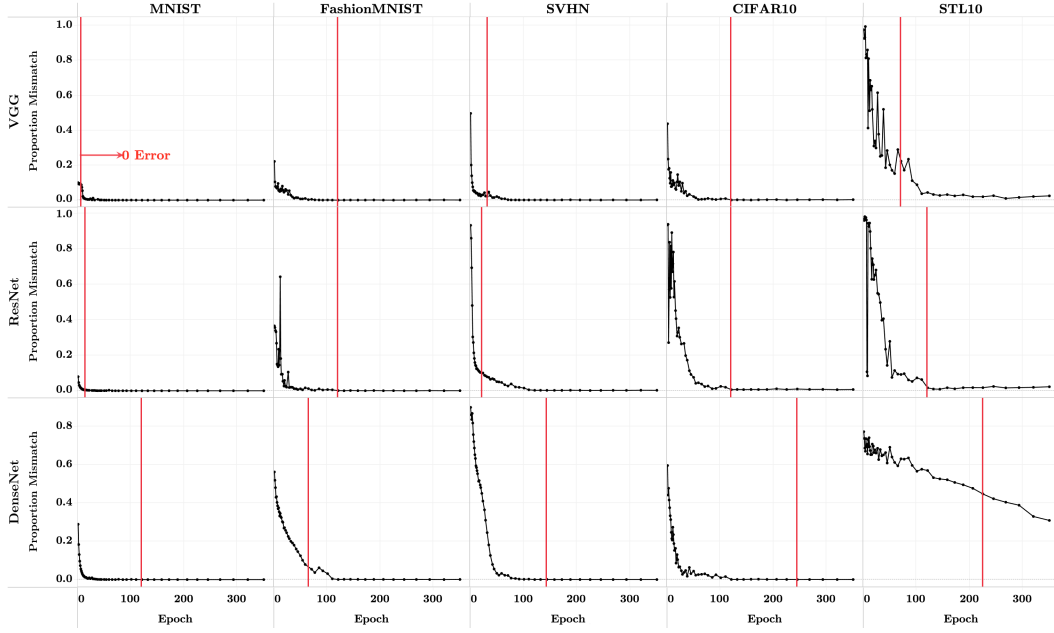


Figure 8: Plots analogous to Figure 7 in Pappan et al. (2020), but on networks trained with MSE Loss. Results demonstrate that classifier decisions converge to those of the *nearest class center decision rule*.

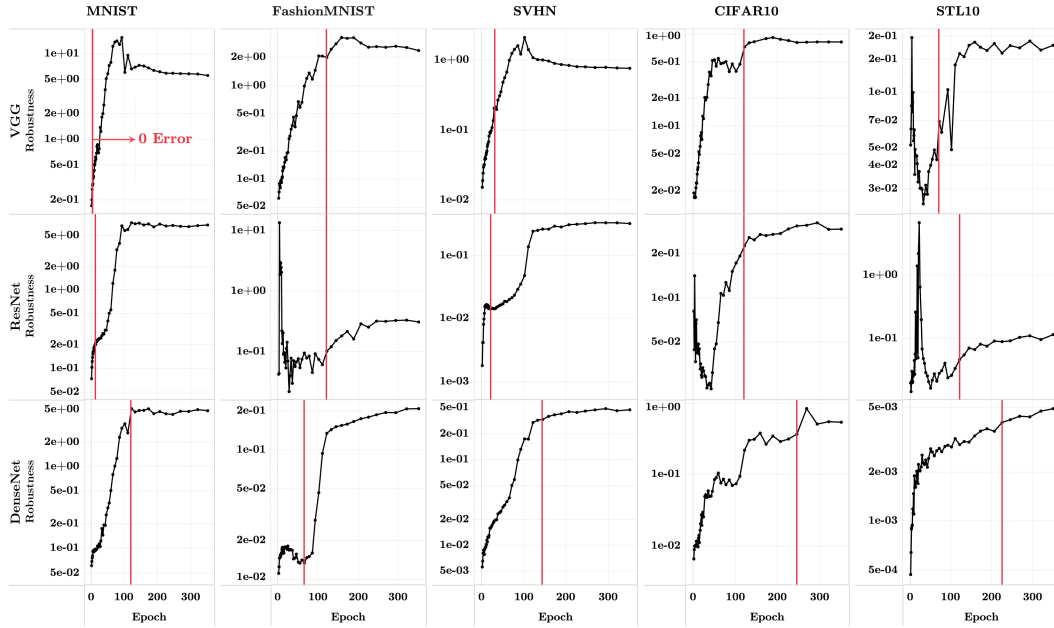


Figure 9: Plots analogous to Figure 8 in Pappan et al. (2020), but on networks trained with MSE Loss. Results demonstrate that networks *become more robust when trained beyond 0-error*. The median improvement in the robustness measure in the last epoch over the first epoch achieving zero training error is 0.1762; the mean improvement is 0.9278.

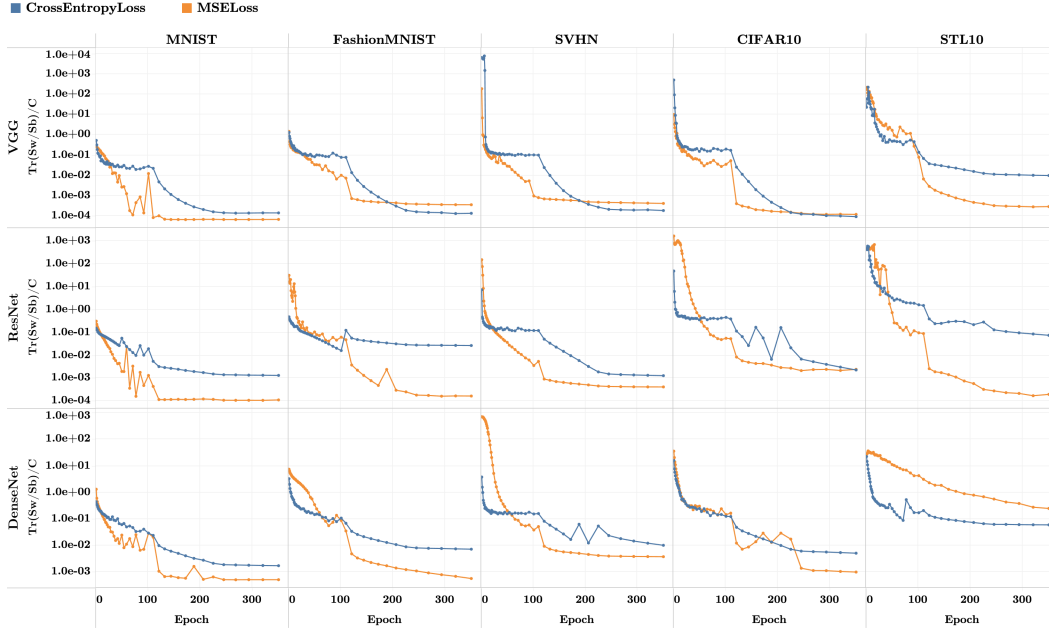


Figure 10: *Activation collapse under MSE loss vs. CE loss*: Comparison of activation collapse observed in this paper for networks trained under MSE loss (Figure 7) with that observed in Papyan et al. (2020) under CE loss. Networks trained with MSE loss tend to achieve faster activation collapse than those trained with CE.

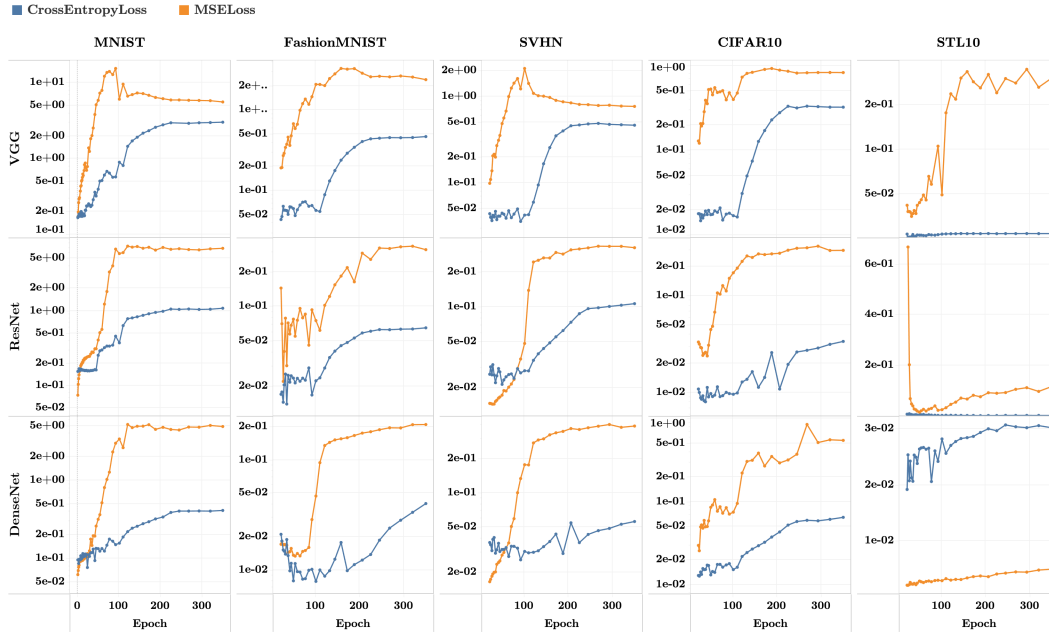


Figure 11: *Adversarial robustness under MSE loss vs. CE loss*: Comparison of adversarial robustness observed in this paper for networks trained under MSE loss (Figure 9) with that observed in Papyan et al. (2020) under CE loss. Robustness tends to be better—sometimes several magnitudes better—when the networks are trained with MSE loss than with CE loss.

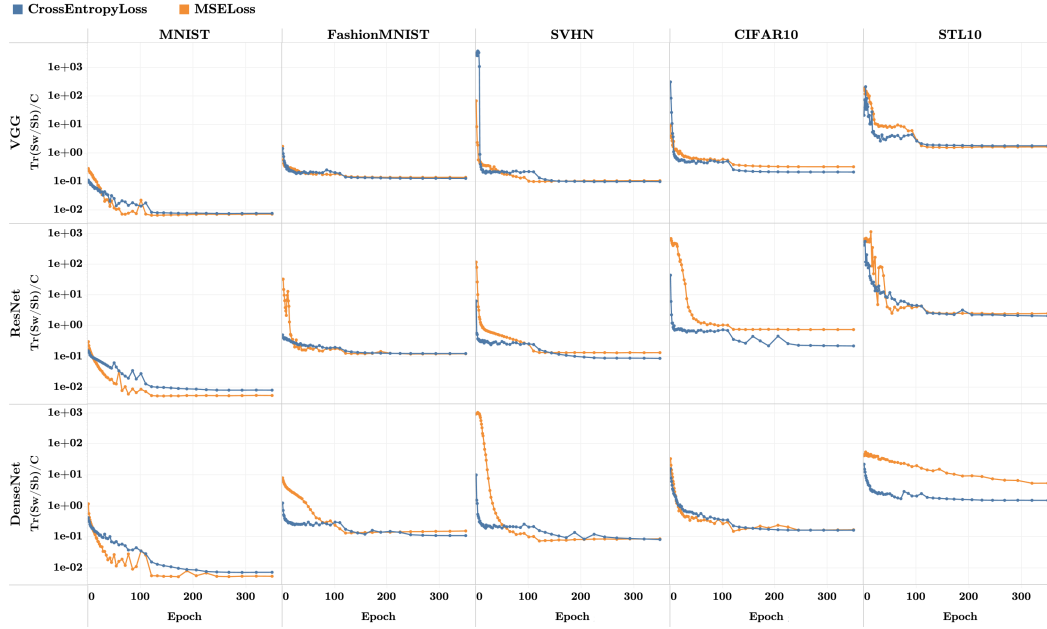


Figure 12: *Activation collapse on test data for both losses:* Activation collapse observed on *test data* for models trained with MSE loss (from this current paper) and CE loss (posted by Pappan, Han, and Donoho (2020) on Stanford Data Repository). On the test data, activation collapse still visibly occurs on multiple dataset-network combinations: Albeit the rate of collapse is much slower on the test data compared to that on the train data, and the plotted measure (described in Figure 6 of Pappan, Han, and Donoho (2020)) at the last epoch is larger than that on the train data. Also interesting is that the value at the last epoch is roughly monotonic with the difficulty of the dataset. See discussion in Section A.8.

A.7 EXCEPTIONS: STL10-RESNET AND STL10-DENSENET

The STL10-ResNet and STL10-DenseNet dataset-network pairs stand out among the experiments described in this section—sometimes displaying outlier behavior either by converging more slowly to Neural Collapse or by exhibiting trends inconsistent with those found in other dataset-network pairs.

STL10 stands apart from the other canonical datasets for multiple reasons¹² and is a “less-typical” benchmark compared to more “compulsory” datasets like CIFAR10. In this particular case, we hypothesize that its outlier behavior might be caused by the size of the STL10 images (96×96 compared to the 32×32 , after padding, of the other datasets)—leading to a higher-dimensional problem, which, in turn, induces a harder non-convex optimization problem, which might make SGD less likely to converge to a useful optimum or might make the convergence much slower and harder to observe under a fixed computational budget.

It was previously noted in Hui & Belkin (2020) and Demirkaya et al. (2020) that more challenging classification problems—in those projects, problems with more classes to be labeled—may require modifications to the MSE loss. We decided that such modifications are unnecessary in the ten class problems examined in this paper’s experiments. But perhaps the outlier nature of the STL10-ResNet and STL10-DenseNet combinations signal that the MSE loss modifications proposed by Hui & Belkin (2020) and Demirkaya et al. (2020) ought to have been used.

A.8 OPEN QUESTIONS: WEIGHT-DECAY, BATCH NORMALIZATION, SGD, GENERALIZATION, TEST DATA

The experiments in this paper as well as those in Papayan, Han, and Donoho (2020) were conducted under the canonical setting where deep nets were trained using SGD with weight-decay and batch normalization—leading one to wonder about the roles that these particular ingredients play on the NC phenomena. Additionally, most observables focus on the train data—raising the question of how the NC phenomena behave on test data as well as their relationship to generalization. We find these questions intriguing, but feel each deserves careful experimentation outside the scope of this paper.

Nonetheless, we note here that several existing papers have already begun insightful investigations in these directions. For example, weight-decay, weight-normalization (as a proxy for batch-normalization), and SGD play key roles in the analyses of Banburski et al. (2019); Poggio & Liao (2020a;b) that, along other things, lead to the prediction of NC in homogeneous deep nets. Banburski et al. (2021) also explores the connection between NC and margin distributions with generalization.

Another example is Zhu et al. (2021) in which the authors conduct several experiments on ResNets trained on CIFAR10. On their models, the authors examine NC-related properties relative to the train data, test data, and randomly labeled data; they also conducted ablation studies varying control parameters (weight-decay, width, etc.) and the optimization algorithm (SGD, ADAM, L-BFGS). Based on their results, Zhu et al. (2021) propose thought-provoking conjectures on the role of each of these components (see Section E.7 for a brief survey of their findings).

As a preliminary exploration, we include Figure 12 showing the variability collapse (**NC1**) behavior on *test data* for the networks trained with MSE loss (used in this paper) as well as those trained with CE loss (released¹³ by Papayan, Han, and Donoho (2020)). From Figure 12, we see that variability collapse occurs much slower on the test data than on the train data. Although not shown here, the other NC phenomena behave similarly.

In this Appendix, we show Figure 12 since it is concise, within reach, and may be of interest to readers who share our curiosity. We refrain from presenting the entire series of multi-figure NC measurements on test data because it is outside the scope of this paper and would significantly lengthen this appendix. We also refrain from speculating on any underlying explanations until more meticulous experiments are conducted.

¹²For example, one sense in which STL-10 is clearly different from the other datasets is the comparatively small number of labeled training examples per class.

¹³The CE test data results were released by Papayan, Han, and Donoho (2020) on the paper’s corresponding Stanford Data Repository entry.

B THEOREM 1

Theorem 1. (Decomposition of MSE Loss) The MSE loss, $\mathcal{L}(\widetilde{\mathbf{W}}, \widetilde{\mathbf{H}})$, can be decomposed into two terms, $\mathcal{L}(\widetilde{\mathbf{W}}, \widetilde{\mathbf{H}}) = \mathcal{L}_{LS}(\widetilde{\mathbf{H}}) + \mathcal{L}_{LS}^\perp(\widetilde{\mathbf{W}}, \widetilde{\mathbf{H}})$, where

$$\mathcal{L}_{LS}(\widetilde{\mathbf{H}}) = \frac{1}{2} \text{Ave}_{i,c} \|\widetilde{\mathbf{W}}_{LS} \widetilde{\mathbf{h}}_{i,c} - \mathbf{y}_{i,c}\|_2^2 + \frac{\lambda}{2} \|\widetilde{\mathbf{W}}_{LS}\|_F^2,$$

and

$$\mathcal{L}_{LS}^\perp(\widetilde{\mathbf{W}}, \widetilde{\mathbf{H}}) = \frac{1}{2} \text{tr} \left\{ (\widetilde{\mathbf{W}} - \widetilde{\mathbf{W}}_{LS}) \left(\widetilde{\boldsymbol{\Sigma}}_T + \widetilde{\boldsymbol{\mu}}_G \widetilde{\boldsymbol{\mu}}_G^\top + \lambda \mathbf{I} \right) (\widetilde{\mathbf{W}} - \widetilde{\mathbf{W}}_{LS})^\top \right\}.$$

Proof. Recall the MSE loss:

$$\mathcal{L}(\widetilde{\mathbf{W}}, \widetilde{\mathbf{H}}) = \frac{1}{2} \text{Ave}_{i,c} \|\widetilde{\mathbf{W}} \widetilde{\mathbf{h}}_{i,c} - \mathbf{y}_{i,c}\|_2^2 + \frac{\lambda}{2} \|\widetilde{\mathbf{W}}\|_F^2. \quad (13)$$

Consider a specific extended activations matrix $\widetilde{\mathbf{H}}$; the least-squares solution $\widetilde{\mathbf{W}}$ minimizing $\mathcal{L}(\widetilde{\mathbf{W}}, \widetilde{\mathbf{H}})$ with $\widetilde{\mathbf{H}}$ kept fixed must obey the following first-order optimality condition:

$$\text{Ave}_{i,c} (\widetilde{\mathbf{W}}_{LS} \widetilde{\mathbf{h}}_{i,c} - \mathbf{y}_{i,c}) \widetilde{\mathbf{h}}_{i,c}^\top + \lambda \widetilde{\mathbf{W}}_{LS} = 0. \quad (14)$$

From Proposition 1 in the main manuscript, the solution to the above is given by

$$\widetilde{\mathbf{W}}_{LS} = \mathbf{C}^{-1} \widetilde{\mathbf{M}}^\top (\widetilde{\boldsymbol{\Sigma}}_T + \lambda \mathbf{I})^{-1}.$$

The loss can be rewritten as

$$\frac{1}{2} \text{Ave}_{i,c} \|\widetilde{\mathbf{W}}_{LS} \widetilde{\mathbf{h}}_{i,c} - \mathbf{y}_{i,c} + (\widetilde{\mathbf{W}} - \widetilde{\mathbf{W}}_{LS}) \widetilde{\mathbf{h}}_{i,c}\|_2^2 + \frac{\lambda}{2} \|\widetilde{\mathbf{W}}\|_F^2.$$

Combining the above with Equation 14 gives, after rearranging:

$$\frac{1}{2} \text{Ave}_{i,c} \|\widetilde{\mathbf{W}}_{LS} \widetilde{\mathbf{h}}_{i,c} - \mathbf{y}_{i,c}\|_2^2 + \frac{1}{2} \text{Ave}_{i,c} \|(\widetilde{\mathbf{W}} - \widetilde{\mathbf{W}}_{LS}) \widetilde{\mathbf{h}}_{i,c}\|_2^2 - \lambda \text{tr} \left\{ \widetilde{\mathbf{W}}_{LS} (\widetilde{\mathbf{W}} - \widetilde{\mathbf{W}}_{LS})^\top \right\} + \frac{\lambda}{2} \|\widetilde{\mathbf{W}}\|_F^2,$$

which is equivalent to

$$\frac{1}{2} \text{Ave}_{i,c} \|\widetilde{\mathbf{W}}_{LS} \widetilde{\mathbf{h}}_{i,c} - \mathbf{y}_{i,c}\|_2^2 + \frac{1}{2} \text{Ave}_{i,c} \|(\widetilde{\mathbf{W}} - \widetilde{\mathbf{W}}_{LS}) \widetilde{\mathbf{h}}_{i,c}\|_2^2 + \frac{\lambda}{2} \|\widetilde{\mathbf{W}}_{LS}\|_F^2 + \frac{\lambda}{2} \|\widetilde{\mathbf{W}}_{LS} - \widetilde{\mathbf{W}}\|_F^2.$$

Using the above, the loss can indeed be decomposed as

$$\mathcal{L}(\widetilde{\mathbf{W}}, \widetilde{\mathbf{H}}) = \mathcal{L}_{LS}(\widetilde{\mathbf{H}}) + \mathcal{L}_{LS}^\perp(\widetilde{\mathbf{W}}, \widetilde{\mathbf{H}}),$$

where

$$\mathcal{L}_{LS}(\widetilde{\mathbf{H}}) \equiv \frac{1}{2} \text{Ave}_{i,c} \|\widetilde{\mathbf{W}}_{LS} \widetilde{\mathbf{h}}_{i,c} - \mathbf{y}_{i,c}\|_2^2 + \frac{\lambda}{2} \|\widetilde{\mathbf{W}}_{LS}\|_F^2 \quad (15)$$

and

$$\begin{aligned} \mathcal{L}_{LS}^\perp(\widetilde{\mathbf{W}}, \widetilde{\mathbf{H}}) &\equiv \frac{1}{2} \text{Ave}_{i,c} \|(\widetilde{\mathbf{W}} - \widetilde{\mathbf{W}}_{LS}) \widetilde{\mathbf{h}}_{i,c}\|_2^2 + \frac{\lambda}{2} \|\widetilde{\mathbf{W}}_{LS} - \widetilde{\mathbf{W}}\|_F^2 \\ &= \frac{1}{2} \text{tr} \left\{ (\widetilde{\mathbf{W}} - \widetilde{\mathbf{W}}_{LS}) \left(\widetilde{\boldsymbol{\Sigma}}_T + \widetilde{\boldsymbol{\mu}}_G \widetilde{\boldsymbol{\mu}}_G^\top + \lambda \mathbf{I} \right) (\widetilde{\mathbf{W}} - \widetilde{\mathbf{W}}_{LS})^\top \right\}. \end{aligned}$$

This completes the proof. \square

C THEOREM 2

Theorem 2. (Decomposition of Central Path Component) The central path component, $\mathcal{L}_{LS}(\widetilde{\mathbf{H}})$, of the MSE decomposition in Theorem 1 can be further decomposed into $\mathcal{L}_{LS}(\widetilde{\mathbf{H}}) = \mathcal{L}_{NC1}(\widetilde{\mathbf{H}}) + \mathcal{L}_{NC2\beta}(\widetilde{\mathbf{H}})$, where

$$\mathcal{L}_{NC1}(\widetilde{\mathbf{H}}) = \frac{1}{2} \text{tr} \left\{ \widetilde{\mathbf{W}}_{LS} \left(\widetilde{\boldsymbol{\Sigma}}_W + \lambda \mathbf{I} \right) \widetilde{\mathbf{W}}_{LS}^\top \right\},$$

and

$$\mathcal{L}_{NC2\beta}(\widetilde{\mathbf{H}}) = \frac{1}{2C} \|\widetilde{\mathbf{W}}_{LS} \widetilde{\mathbf{M}} - \mathbf{I}\|_F^2.$$

Proof. Under Euclidean distance, perturbations to the extended activations matrix $\widetilde{\mathbf{H}}$ which affect only the class-means or global-mean are *orthogonal* to perturbations which affect only the within-class covariance. Using this, $\mathcal{L}_{\text{LS}}(\widetilde{\mathbf{H}})$ can be further decomposed via the Pythagorean theorem:

$$\mathcal{L}_{\text{LS}}(\widetilde{\mathbf{H}}) = \frac{1}{2} \text{Ave}_{i,c} \|\widetilde{\mathbf{W}}_{\text{LS}}(\widetilde{\mathbf{h}}_{i,c} - \widetilde{\boldsymbol{\mu}}_c)\|_2^2 + \frac{\lambda}{2} \|\widetilde{\mathbf{W}}_{\text{LS}}\|_F^2 + \frac{1}{2} \text{Ave}_c \|\widetilde{\mathbf{W}}_{\text{LS}}\widetilde{\boldsymbol{\mu}}_c - \mathbf{y}_{i,c}\|_2^2.$$

The first and second terms above merge into $\mathcal{L}_{\text{NC1}}(\widetilde{\mathbf{H}})$, while the third term becomes $\mathcal{L}_{\text{NC2/3}}(\widetilde{\mathbf{H}})$:

$$\begin{aligned} \mathcal{L}_{\text{NC1}}(\widetilde{\mathbf{H}}) &= \frac{1}{2} \text{tr} \left\{ \widetilde{\mathbf{W}}_{\text{LS}} \left(\widetilde{\boldsymbol{\Sigma}}_W + \lambda \mathbf{I} \right) \widetilde{\mathbf{W}}_{\text{LS}}^\top \right\} \\ \mathcal{L}_{\text{NC2/3}}(\widetilde{\mathbf{H}}) &= \frac{1}{2C} \|\widetilde{\mathbf{W}}_{\text{LS}}\widetilde{\mathbf{M}} - \mathbf{I}\|_F^2. \end{aligned} \quad (16)$$

This completes the proof. \square

C.1 INTUITIONS FOR THEOREM 2 IN UNEXTENDED COORDINATES

For intuition, consider when $\lambda = 0$, i.e. the no weight-decay case. Proposition 1 in the main text gives

$$\mathbf{W}_{\text{LS}} = \mathbf{C}^{-1} \overline{\mathbf{M}}^\top \boldsymbol{\Sigma}_T^{-1}, \quad (17)$$

where $\overline{\mathbf{M}} \in \mathbb{R}^{P \times C}$ is the matrix with columns $\boldsymbol{\mu}_c - \boldsymbol{\mu}_G$. Returning to the unextended coordinates, $\mathcal{L}_{\text{NC1}}(\overline{\mathbf{H}})$ simplifies to

$$\mathcal{L}_{\text{NC1}}(\overline{\mathbf{H}}) = \frac{1}{2} \text{tr} \{ \mathbf{W}_{\text{LS}} \boldsymbol{\Sigma}_W \mathbf{W}_{\text{LS}}^\top \}, \quad (18)$$

where $\overline{\mathbf{H}} \in \mathbb{R}^{P \times CN}$ has columns $\mathbf{h}_{i,c} - \boldsymbol{\mu}_G$. The term $\mathcal{L}_{\text{NC2/3}}(\overline{\mathbf{H}})$ also simplifies instructively to

$$\mathcal{L}_{\text{NC2/3}}(\overline{\mathbf{H}}) = \frac{1}{2C} \|\mathbf{W}_{\text{LS}}\overline{\mathbf{M}} - \boldsymbol{\Phi}\|_F^2, \quad (19)$$

where $\boldsymbol{\Phi} \in \mathbb{R}^{C \times C}$ is the standard Simplex ETF:

$$\boldsymbol{\Phi} = \mathbf{I} - \frac{1}{C} \mathbf{1}\mathbf{1}^\top.$$

C.2 ADDITIONAL INTUITIONS FOR THEOREM 2 TERMS

The expressions in Equation 16 and Equation 18 further evoke the intuition that

$\mathcal{L}_{\text{NC1}}(\overline{\mathbf{H}})$ is a variance term that goes to zero only under activation collapse (NC1)

More specifically, we see that, *with the class-means held constant*, the only way to have $\mathcal{L}_{\text{NC1}}(\overline{\mathbf{H}}) \rightarrow 0$ is for $\boldsymbol{\Sigma}_W \rightarrow \mathbf{0}$. Similarly, by examining Equation 19, we see that

$\mathcal{L}_{\text{NC2/3}}(\overline{\mathbf{H}})$ quantifies deviations of $\mathbf{W}_{\text{LS}}\overline{\mathbf{M}}$ —i.e. the matrix of class-mean predictions—from the standard Simplex ETF.

Under (NC2) and (NC3), both \mathbf{W}_{LS} and $\overline{\mathbf{M}}$ tend to jointly aligned ETF's, possibly in an alternate pose; so $\mathbf{W}_{\text{LS}} \rightarrow \boldsymbol{\Phi} \mathbf{U}^T$ and $\overline{\mathbf{M}} \rightarrow \mathbf{U} \boldsymbol{\Phi}$ for a partial orthogonal matrix \mathbf{U} satisfying $\mathbf{U}^T \mathbf{U} = \mathbf{I}_C$. Since $\boldsymbol{\Phi}^2 = \boldsymbol{\Phi}$, (NC2) and (NC3) together demand $\mathbf{W}_{\text{LS}}\overline{\mathbf{M}} \rightarrow \boldsymbol{\Phi}$. Thus, $\mathcal{L}_{\text{NC2/3}}(\overline{\mathbf{H}})$ can be interpreted as a semi-metric reflecting the distance from achieving (NC2) and (NC3).

D THEOREM 3

D.1 IMPLICATIONS OF INVARIANCE

In this section, we will discuss in more detail how the invariance observed Section 3.1 leads to the continually renormalized gradient flow (Equation 5). In particular, we have seen in Section 3.1 of the main text that, on the central path, both the predictions $\mathbf{W}_{\text{LS}}(\overline{\mathbf{H}})\overline{\mathbf{H}}$ and the MSE loss

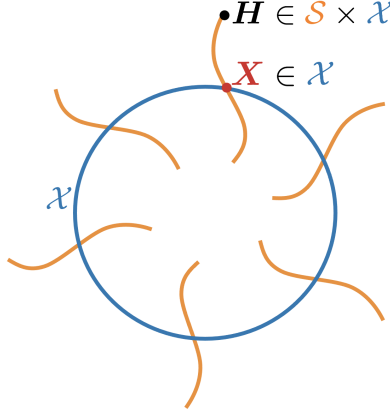


Figure 13: *Fiber bundle*. Any full-rank features matrix, $\bar{\mathbf{H}}$, has a representative element, \mathbf{X} , on \mathcal{X} . For any $\mathbf{X} \in \mathcal{X}$, a *fiber* is the set $\mathcal{S} \times \mathbf{X}$ i.e. $\{\mathbf{A}\mathbf{X} : \mathbf{A} \in \mathcal{S}\}$ (the Minkowski set product), where \mathcal{S} is the set of symmetric positive-definite matrices. Features on the same fiber generate the *same* class predictions and the *same* MSE loss. The optimization described in Sections D.1-D.3 moves *fiber-to-fiber*.

$\mathcal{L}(\mathbf{W}_{\text{LS}}(\bar{\mathbf{H}}), \bar{\mathbf{M}}(\bar{\mathbf{H}}))$ are invariant under the transformation $\bar{\mathbf{H}} \mapsto \mathbf{A}\bar{\mathbf{H}}$ when \mathbf{A} is an invertible matrix. Since our interest mainly lies with $\mathbf{A} = \Sigma_W^{-\frac{1}{2}}$, we will restrict the intuitive discussion in this section to positive-definite \mathbf{A} .

Now, consider the set \mathcal{H} of features $\bar{\mathbf{H}}$ with non-singular within-class covariances. We view \mathcal{H} as a fiber bundle¹⁴, where—on each fiber—live (apparently) different activations, $\bar{\mathbf{H}}$, that (in fact) generate the exact *same* class predictions and the exact *same* MSE loss (see Figure 13). The base space—we will denote it \mathcal{X} —can be taken to be the collection of $\mathbf{X} \in \mathcal{H}$ where $\Sigma_W(\mathbf{X}) = \mathbf{I}$. Every $\bar{\mathbf{H}} \in \mathcal{H}$ is representable as $\bar{\mathbf{H}} = \mathbf{A}\mathbf{X}$ where $\mathbf{A} = \Sigma_W^{-\frac{1}{2}}(\bar{\mathbf{H}})$ and $\Sigma_W(\mathbf{X}) = \mathbf{I}$. The activation matrices \mathbf{X} in the base space might be variously called “pre-whitened,” “normalized,” “standardized,” or “sphered.” We shall call \mathcal{X} a *normalized features manifold*¹⁵.

Invoking invariance, we can make the following observations about our optimization task:

1. If, at a specific t , \mathbf{H}_t happens to be a normalized set of activations (i.e. $\mathbf{H}_t \in \mathcal{X}$ is currently located in the base space \mathcal{X}), there is no performance benefit to leaving the base space. There is also *no performance benefit* to moving *along* a fiber; only by moving from *fiber-to-fiber* can we improve performance.
2. In some sense, we waste time *except* when jumping from fiber-to-fiber; we might prefer to stay in the base space all the time by forcing the dynamics to jump from fiber-to-fiber.

On the other hand, we started with the viewpoint of studying gradient flow of the original \mathbf{H} . So, we consider the following natural model for the application of gradient descent in \mathbf{X} :

1. For a given initial feature activations, $\bar{\mathbf{H}}_0 \in \mathcal{H}$, we renormalize—obtaining a starting point $\mathbf{X}_0 \in \mathcal{X}$; here $\mathbf{X}_0 = \Sigma_W^{-\frac{1}{2}}(\bar{\mathbf{H}}_0)\bar{\mathbf{H}}_0$. Class predictions and MSE loss performance for the MSE-optimal classifier do not change from this renormalization.
2. We compute the usual gradient of MSE loss, at \mathbf{X}_0 , obtaining a step $\Delta\mathbf{X}_0 = -\eta\nabla_{\mathbf{X}}\mathcal{L}_{\text{LS}}(\mathbf{X}_0)$, where η is a step size.
3. We take a step, going to

$$\bar{\mathbf{H}}_1 = \mathbf{X}_0 + \Delta\mathbf{X}_0.$$

¹⁴An even larger space could be considered, where $\Sigma_W(\bar{\mathbf{H}})$ is not necessarily full rank, and then other components of this space having covariances of rank C , $C - 1, \dots, 1$ could be considered. We just discuss the full-rank case here.

¹⁵This is sometimes called the *Generalized Stiefel Manifold* and will be defined more formally in Section D.2.

4. $\bar{\mathbf{H}}_1$ will not necessarily be normalized. We map back along whatever fiber we have landed upon, obtaining a corresponding point in the base space \mathcal{X} , call this \mathbf{X}_1 . Here,

$$\mathbf{X}_1 = \Sigma_W^{-\frac{1}{2}}(\bar{\mathbf{H}}_1)\bar{\mathbf{H}}_1.$$

Class predictions and MSE loss performance do not change from this renormalization.

5. Repeat steps 2, 3, 4 at \mathbf{X}_1 , obtaining thereby \mathbf{X}_2 ; and so on.

This process might be described as *gradient descent with continual renormalization*:

1. Renormalize the initial features activation matrix;
2. Compute the ordinary gradient of MSE loss and take the gradient descent step;
3. Renormalize again after each such step; and
4. Repeat steps 2 and 3.

While the continual renormalization process differs from usual gradient flow, it is both intuitively understandable and sensible. See discussion of assumption **(A3)** in Section 3

D.2 ALIGNED SNR COORDINATES

Analysis of continually renormalized gradient flow can be simplified, without loss of generality, by applying a change of basis in both row and column space:

Definition 3 (Transformation into Aligned SNR Coordinates). Consider the SVD decomposition of the SNR from Definition 2 outputting left singular vectors $\mathbf{U} \in \mathbb{R}^{P \times C}$ and right singular vectors $\mathbf{V} \in \mathbb{R}^{C \times C}$. For any matrix $\mathbf{Z} \in \mathbb{R}^{P \times C}$, define the transformation $\mathbf{Z} \rightarrow \mathbf{U}^\top \mathbf{Z} \mathbf{V}$ as the *transformation into aligned-SNR coordinates*.

The aligned-SNR coordinates is so-named because it diagonalizes i.e. aligns the SNR matrix:

Definition 4 (Aligned SNR Matrix). Consider the SVD decomposition of the SNR from Definition 2. Combined with Equation 9, observe that

$$\mathbf{\Omega} = \text{diag}(\{\omega_c\}_{c=1}^{C-1}, 0) = \mathbf{U}^\top \Sigma_W^{-\frac{1}{2}} \bar{\mathbf{M}} \mathbf{V}$$

We call $\mathbf{\Omega}$ the *aligned SNR matrix*.

The following facts about the aligned SNR matrix becomes useful later in our derivations:

Observation 1 (SVD of Aligned SNR Matrix). The SVD of the aligned SNR matrix itself is simply

$$\mathbf{\Omega} = \sum_{j=1}^{C-1} \omega_j \mathbf{e}_j \mathbf{e}_j^\top,$$

with the canonical basis $\{\mathbf{e}_j\}_{j=1}^C$ as its singular vectors.

As discussed in Section 3.2, the $\{\omega_c\}_{c=1}^{C-1}$ that comprise $\mathbf{\Omega}$ are decisive for understanding separation performance. In fact, the MSE loss can be entirely characterized by the SNR singular values on the central path:

Lemma 1 (Spectral Representation of MSE Loss). On the central path, the MSE loss obeys

$$\mathcal{L}(\mathbf{W}_{LS}(\bar{\mathbf{H}}), \bar{\mathbf{H}}) = \mathcal{L}_{LS}(\mathbf{W}_{LS}(\bar{\mathbf{H}}), \bar{\mathbf{H}}) = \frac{1}{2} \sum_{j=1}^{C-1} \frac{1}{\omega_j^2 + C} = \mathcal{L}(\{\omega_j\}_{j=1}^{C-1}),$$

and its decomposition obeys

$$\begin{aligned} \mathcal{L}_{NCI}(\bar{\mathbf{H}}) &= \frac{1}{2} \sum_{j=1}^{C-1} \frac{\omega_j^2}{(C + \omega_j^2)^2} = \mathcal{L}_{NCI}(\{\omega_j\}_{j=1}^{C-1}) \\ \mathcal{L}_{NC2/3}(\bar{\mathbf{H}}) &= \frac{1}{2} \sum_{j=1}^{C-1} \frac{1}{C} \left(\frac{\omega_j^2}{\omega_j^2 + C} - 1 \right)^2 = \mathcal{L}_{NC2/3}(\{\omega_j\}_{j=1}^{C-1}). \end{aligned}$$

Proof. Using Equation 17, Equation 18, and Equation 19, the loss on the central path equals

$$\mathcal{L}(\mathbf{W}_{\text{LS}}, \bar{\mathbf{M}}) = \frac{1}{2C} \|C^{-1} \bar{\mathbf{M}}^\top \Sigma_T^{-1} \bar{\mathbf{M}} - \Phi\|_F^2 + \frac{1}{2} \text{tr}\{C^{-1} \bar{\mathbf{M}}^\top \Sigma_T^{-1} \Sigma_W \Sigma_T^{-1} \bar{\mathbf{M}} C^{-1}\}. \quad (20)$$

Observe $\bar{\mathbf{M}}^\top \Sigma_T^{-1} \bar{\mathbf{M}}$ and Φ are simultaneously diagonalizable since they share the same $[1, \dots, 1]^\top$ null space and Φ has $C - 1$ equal eigenvalues. Also, observe that

$$\Sigma_T = \Sigma_W + \frac{1}{C} \bar{\mathbf{M}} \bar{\mathbf{M}}^\top.$$

Let $\hat{\Omega}$ be submatrix of the aligned-SNR matrix Ω corresponding to the non-zero singular values i.e. $\hat{\Omega} = \text{diag}(\{\omega_j\}_{j=1}^{C-1})$. After taking simultaneous-diagonalizations and canceling partial orthogonal matrices, Equation 20 can be written solely in terms of $\hat{\Omega}$:

$$\mathcal{L}(\hat{\Omega}) = \frac{1}{2C} \left\| \hat{\Omega}^\top (\hat{\Omega} \hat{\Omega}^\top + C \mathbf{I}_{C-1})^{-1} \hat{\Omega} - \mathbf{I}_{C-1} \right\|_F^2 + \frac{1}{2} \text{tr}\{\hat{\Omega}^\top (\hat{\Omega} \hat{\Omega}^\top + C \mathbf{I}_{C-1})^{-2} \hat{\Omega}\}.$$

This can be further simplified into

$$\begin{aligned} \mathcal{L}(\{\omega_j\}_{j=1}^{C-1}) &= \frac{1}{2} \sum_{j=1}^{C-1} \frac{1}{C} \left(\frac{\omega_j^2}{\omega_j^2 + C} - 1 \right)^2 + \frac{\omega_j^2}{(C + \omega_j^2)^2} \\ &= \frac{1}{2} \sum_{j=1}^{C-1} \frac{1}{\omega_j^2 + C}. \end{aligned} \quad (21)$$

This completes the proof for Lemma 1. \square

Thus, the aligned SNR matrix, $\mathbf{U}^\top \Sigma_W^{-\frac{1}{2}} \bar{\mathbf{M}} \mathbf{V}$, maximally simplifies analysis by reducing the vanilla SNR matrix to a diagonal matrix (Definition 4) whose entries determine the MSE loss (Lemma 1).

We introduce the alignment of features into their own notion of aligned SNR coordinates:

Definition 5 (Renormalization to aligned SNR Coordinates). Consider $\bar{\mathbf{H}} \in \mathbb{R}^{P \times CN}$ with corresponding SNR left and right singular vectors \mathbf{U} and \mathbf{V} (Definition 2). Then, define the SNR-aligned renormalization of the features as

$$\mathbf{X} = \mathbf{U}^\top (\Sigma_W)^{-\frac{1}{2}} \bar{\mathbf{H}} (\mathbf{V} \otimes \mathbf{I}_N) = \mathbf{U}^\top (\bar{\mathbf{H}} \mathbf{C} \bar{\mathbf{H}}^\top)^{-\frac{1}{2}} \bar{\mathbf{H}} (\mathbf{V} \otimes \mathbf{I}_N) \in \mathbb{R}^{C \times NC},$$

where \otimes is the Kronecker product and \mathbf{C} is a class-centering matrix defined as

$$\mathbf{C} = \frac{1}{CN} \left(\mathbf{I}_{CN} - \frac{1}{N} \mathbf{Y}^\top \mathbf{Y} \right). \quad (22)$$

As discussed in Section 3.1, the transformation $\bar{\mathbf{H}} \rightarrow \Sigma_W^{-\frac{1}{2}} \bar{\mathbf{H}}$ does not change the predictions of the least squares classifier. Hence, it does not change the MSE loss. It is easy to check that this still holds for \mathbf{X} i.e. invariance is preserved by the change into SNR-aligned coordinates.

It is easy to check that the sphericity of the within-class covariance is preserved as well:

Observation 2 (Sphericity of Within-Class Covariance of SNR Coordinates).

$$\mathbf{X} \mathbf{C} \mathbf{X}^\top = \mathbf{I}_C$$

It is easy to check by applying Definitions and canceling out (partial) orthogonal matrix multiplications that transforming to aligned SNR coordinates leads to the following simple representations for Ω and its differential:

Observation 3 (Relation Between SNR Coordinates and SNR Matrix). The aligned SNR matrix, Ω (Definition 4) can be expressed as a function of the features in aligned SNR-coordinates \mathbf{X} (Definition 5) as simply

$$\Omega(\mathbf{X}) = \frac{1}{N} \mathbf{X} \mathbf{Y}^\top.$$

Moreover, let $d\Omega_{ij}(\cdot) : T_{\mathbf{X}}\mathcal{X} \rightarrow \mathbb{R}$ be the differential 1-form¹⁶ associated with the ij -th entry of Ω . Define $d\Omega(\cdot) : T_{\mathbf{X}}\mathcal{X} \rightarrow \mathbb{R}^{C \times C}$ such that, for some $\mathbf{Z} \in T_{\mathbf{X}}\mathcal{X}$, each entry matrix of the matrix $d\Omega(\mathbf{Z})$ is $d\Omega_{i,j}(\mathbf{Z})$. Then, it follows that

$$d\Omega(\mathbf{Z}) = \frac{1}{N} \mathbf{Z} \mathbf{Y}^\top, \quad \forall \mathbf{Z} \in T_{\mathbf{X}}\mathcal{X}.$$

From a geometric perspective, the transformation in Definition 5 maps the features, \mathbf{H} , to \mathbf{X} belonging to a *Normalized Features Manifold*:

Definition 6 (Normalized Features Manifold).

$$\mathcal{X} = \{\mathbf{X} \in \mathbb{R}^{C \times CN} \mid \mathbf{X} \mathbf{C} \mathbf{X}^\top = \mathbf{I}_C\}$$

To understand the dynamics of the singular values of Ω —which is connected to the dynamics of the features through Lemma 1—we will analyze the gradient flow *on this manifold*. To this end, we first identify its tangent space at a particular \mathbf{X} as well as the projection operator onto that tangent space.

Proposition 3 (Tangent Space of Normalized Features Manifold).

$$T_{\mathbf{X}}\mathcal{X} = \{\mathbf{Z} \in \mathbb{R}^{C \times CN} \mid \mathbf{X} \mathbf{C} \mathbf{Z}^\top + \mathbf{Z} \mathbf{C} \mathbf{X} = \mathbf{0}\}$$

Proposition 4 (Projection Onto Tangent Space of Normalized Features Manifold).

$$\Pi_{T_{\mathbf{X}}\mathcal{X}}(\mathbf{Z}) = \mathbf{Z} - \frac{1}{2}(\mathbf{X} \mathbf{C} \mathbf{Z}^\top + \mathbf{Z} \mathbf{C} \mathbf{X}^\top) \mathbf{X}$$

D.3 CONTINUALLY RENORMALIZED GRADIENT FLOW

In fact, gradient flow on the normalized features manifold (Definition 6) is the continuous analogue of the intuitive, discrete algorithm in Subsection D.1. In particular, the intuitive algorithm consists of a gradient step, $\bar{\mathbf{H}}_1 = \mathbf{X}_0 + \Delta \mathbf{X}_0$ followed by a mapping to the base space of the fiber bundle, $\mathbf{X}_1 = \Sigma(\bar{\mathbf{H}}_1)^{-\frac{1}{2}} \bar{\mathbf{H}}_1$. For small $\Delta \mathbf{X}_0$, these two steps are in fact equivalent (up to a negligible term) to taking a $T_{\mathbf{X}}\mathcal{X}$ -projected gradient step on the manifold \mathcal{X} as proven below:

Lemma 2. Assuming $\mathbf{X}_0 \in \mathcal{X}$, a renormalized gradient step,

$$\mathbf{X}_1 = \Sigma_W^{-\frac{1}{2}}(\bar{\mathbf{H}}_1) \bar{\mathbf{H}}_1 = \Sigma_W^{-\frac{1}{2}}(\mathbf{X}_0 + \Delta \mathbf{X}_0) \cdot (\mathbf{X}_0 + \Delta \mathbf{X}_0),$$

is equivalent, up to an $O(\|\Delta \mathbf{X}_0\|^2)$ term, to a $T_{\mathbf{X}}\mathcal{X}$ -projected gradient step, i.e.

$$\mathbf{X}_1 = \mathbf{X}_0 + \Pi_{T_{\mathbf{X}}\mathcal{X}}(\Delta \mathbf{X}_0) + O(\|\Delta \mathbf{X}_0\|^2).$$

Proof. Notice that

$$\begin{aligned} \mathbf{X}_1 &= \Sigma_W^{-\frac{1}{2}}(\bar{\mathbf{H}}_1) \bar{\mathbf{H}}_1 \\ &= ((\mathbf{X}_0 + \Delta \mathbf{X}_0) \mathbf{C} (\mathbf{X}_0 + \Delta \mathbf{X}_0)^\top)^{-\frac{1}{2}} (\mathbf{X}_0 + \Delta \mathbf{X}_0) \\ &= (\mathbf{I} + \Delta \mathbf{X}_0 \mathbf{C} \mathbf{X}_0^\top + \mathbf{X}_0 \mathbf{C} \Delta \mathbf{X}_0^\top + \Delta \mathbf{X}_0 \mathbf{C} \Delta \mathbf{X}_0^\top)^{-\frac{1}{2}} (\mathbf{X}_0 + \Delta \mathbf{X}_0), \end{aligned}$$

where in the last step we used our assumption that $\mathbf{X}_0 \in \mathcal{X}$, i.e., $\mathbf{X}_0 \mathbf{C} \mathbf{X}_0 = \mathbf{I}$. By Taylor's Theorem,

$$(\mathbf{I} + \mathbf{A})^{-\frac{1}{2}} = \mathbf{I} - \frac{1}{2} \mathbf{A} + O(\|\mathbf{A}\|^2).$$

Therefore, we get

$$\begin{aligned} \mathbf{X}_1 &= \left(\mathbf{I} - \frac{1}{2} (\Delta \mathbf{X}_0 \mathbf{C} \mathbf{X}_0^\top + \mathbf{X}_0 \mathbf{C} \Delta \mathbf{X}_0^\top + \Delta \mathbf{X}_0 \mathbf{C} \Delta \mathbf{X}_0^\top) + O(\|\Delta \mathbf{X}_0\|^2) \right) (\mathbf{X}_0 + \Delta \mathbf{X}_0) \\ &= \mathbf{X}_0 + \Delta \mathbf{X}_0 - \frac{1}{2} (\Delta \mathbf{X}_0 \mathbf{C} \mathbf{X}_0^\top + \mathbf{X}_0 \mathbf{C} \Delta \mathbf{X}_0^\top) \mathbf{X}_0 + O(\|\Delta \mathbf{X}_0\|^2) \\ &= \mathbf{X}_0 + \Pi_{T_{\mathbf{X}}\mathcal{X}}(\Delta \mathbf{X}_0) + O(\|\Delta \mathbf{X}_0\|^2), \end{aligned}$$

where the last step follows from Proposition 4. \square

As we transition from a discrete gradient descent to a continuous gradient flow, the step size $\eta \rightarrow 0$, and the residual $O(\|\Delta \mathbf{X}_0\|^2)$ in the above lemma becomes negligible, since $\Delta \mathbf{X}_0 = -\eta \nabla_{\mathbf{X}} \mathcal{L}_{\text{LS}}(\mathbf{X}_0)$. This motivates us to study, in the next section, the continually renormalized gradient flow (as defined in Equation 5 of the main text) of \mathbf{X} on \mathcal{X} :

$$\frac{d}{dt} \mathbf{X} = -\Pi_{T_{\mathbf{X}} \mathcal{X}} (\nabla_{\mathbf{X}} \mathcal{L}_{\text{LS}}(\mathbf{X})).$$

D.4 PROOF OF PROPOSITION 2 (GRADIENT FLOW IN ALIGNED SNR COORDINATES)

To prove Proposition 2, we first set up some auxiliary notation and lemmas. Denote the j -th row (transposed) of \mathbf{X} and \mathbf{Y} , respectively, by

$$\mathbf{x}_j = \mathbf{X}^\top \mathbf{e}_j \quad (23)$$

and

$$\mathbf{y}_j = \mathbf{Y}^\top \mathbf{e}_j.$$

Recall that—when differentiating SVDs—the derivative of the j -th singular value, ω_j , only depends on the j -th singular subspace (see Equation 17 of Townsend (2016)). As a consequence, we will see in the following lemma that, for any differential $d\mathbf{X}$, the corresponding $d\omega_j$ only depends on $d\mathbf{x}_j$.

Lemma 3 (Derivative of Singular Values With Respect to SNR Coordinates). *Given the differential 1-form $d\omega_j(\cdot) : T_{\mathbf{X}} \mathcal{X} \rightarrow \mathbb{R}$, the following holds for all¹⁶ $d\mathbf{X} \in \mathbb{R}^{C \times CN}$:*

$$d\omega_j(\Pi_{T_{\mathbf{X}} \mathcal{X}}(d\mathbf{X})) = \left(\frac{1}{N} \mathbf{y}_j^\top - \omega_j \mathbf{x}_j^\top \mathbf{C} \right) d\mathbf{x}_j, \quad \forall j = 1, \dots, C-1.$$

where $\Pi_{T_{\mathbf{X}} \mathcal{X}}$ denotes the projection onto the tangent space of \mathcal{X} at \mathbf{X} .

Proof. Using Observation 1 and the differential of the singular value decomposition (see Equation 17 of Townsend (2016)):

$$d\omega_j(\Pi_{T_{\mathbf{X}} \mathcal{X}}(d\mathbf{X})) = \mathbf{e}_j^\top d\boldsymbol{\Omega}(\Pi_{T_{\mathbf{X}} \mathcal{X}}(d\mathbf{X})) \mathbf{e}_j, \quad (24)$$

where $d\boldsymbol{\Omega}(\cdot)$ is defined as in Observation 3. Next, Observation 3 implies

$$d\boldsymbol{\Omega}(\Pi_{T_{\mathbf{X}} \mathcal{X}}(d\mathbf{X})) = \frac{1}{N} \Pi_{T_{\mathbf{X}} \mathcal{X}}(d\mathbf{X}) \mathbf{Y}^\top. \quad (25)$$

Using the projection onto the tangent space, given in Proposition 4 above,

$$\Pi_{T_{\mathbf{X}} \mathcal{X}}(d\mathbf{X}) = d\mathbf{X} - \frac{1}{2} (d\mathbf{X} \mathbf{C} \mathbf{X}^\top + \mathbf{X} \mathbf{C} d\mathbf{X}^\top) \mathbf{X}. \quad (26)$$

Combining Equation 24, Equation 25, and Equation 26, we obtain:

$$\begin{aligned} d\omega_j(\Pi_{T_{\mathbf{X}} \mathcal{X}}(d\mathbf{X})) &= \mathbf{e}_j^\top d\boldsymbol{\Omega}(\Pi_{T_{\mathbf{X}} \mathcal{X}}(d\mathbf{X})) \mathbf{e}_j \\ &= \frac{1}{N} \mathbf{e}_j^\top \Pi_{T_{\mathbf{X}} \mathcal{X}}(d\mathbf{X}) \mathbf{Y}^\top \mathbf{e}_j \\ &= \frac{1}{N} \mathbf{e}_j^\top \left(d\mathbf{X} - \frac{1}{2} (d\mathbf{X} \mathbf{C} \mathbf{X}^\top + \mathbf{X} \mathbf{C} d\mathbf{X}^\top) \mathbf{X} \right) \mathbf{Y}^\top \mathbf{e}_j. \end{aligned} \quad (27)$$

¹⁶Notation: For real-valued functions f , we use $df(\cdot) : T_{\mathbf{X}} \mathcal{X} \rightarrow \mathbb{R}$ to denote associated the differential 1-form i.e. the function outputting the directional derivative of f in the direction of the argument; For matrices $\mathbf{Z} \in \mathbb{R}^{m \times n}$, we use $d\mathbf{Z} \in \mathbb{R}^{m \times n}$ —without succeeding parenthesis—to denote the matrix differential (cf. Townsend (2016)). These notions are equivalent: $df(\cdot)$ can be represented as a vector $d\mathbf{f}$ in the dual-space of $T_{\mathbf{X}} \mathcal{X}$; When \mathbf{Z} is a function of some vector \mathbf{v} , $d\mathbf{Z}$ can be represented as a collection of 1-forms by defining $d\mathbf{Z}_{ij}(\cdot) = \left\langle \frac{d\mathbf{Z}_{ij}}{d\mathbf{v}}, \cdot \right\rangle$ for each entry \mathbf{Z}_{ij} .

Moreover, using Observation 1 and 3, we can simplify these expressions into

$$\begin{aligned}\frac{1}{N} \mathbf{e}_j^\top d\mathbf{X} \mathbf{Y}^\top \mathbf{e}_j &= \frac{1}{N} \mathbf{y}_j^\top d\mathbf{x}_j \\ \frac{1}{N} \mathbf{e}_j^\top d\mathbf{X} \mathbf{C} \mathbf{X}^\top \mathbf{X} \mathbf{Y}^\top \mathbf{e}_j &= \omega_j \mathbf{e}_j^\top d\mathbf{X} \mathbf{C} \mathbf{X}^\top \mathbf{e}_j = \omega_j \mathbf{x}_j^\top \mathbf{C} d\mathbf{x}_j \\ \frac{1}{N} \mathbf{e}_j^\top \mathbf{X} \mathbf{C} d\mathbf{X}^\top \mathbf{X} \mathbf{Y}^\top \mathbf{e}_j &= \omega_j \mathbf{e}_j^\top \mathbf{X} \mathbf{C} d\mathbf{X}^\top \mathbf{e}_j = \omega_j \mathbf{x}_j^\top \mathbf{C} d\mathbf{x}_j.\end{aligned}$$

Finally, substituting the above three expressions into Equation 27, we get:

$$d\omega_j (\Pi_{T_{\mathbf{X}} \mathcal{X}}(d\mathbf{X})) = \left(\frac{1}{N} \mathbf{y}_j^\top - \omega_j \mathbf{x}_j^\top \mathbf{C} \right) d\mathbf{x}_j,$$

which proves the claim. \square

Using Lemma 3, we can now obtain the dynamics of \mathbf{x}_j under gradient flow:

Lemma 4. *Under continually renormalized gradient flow (Equation 5),*

$$\frac{d}{dt} \mathbf{x}_j = \frac{\omega_j}{(C + \omega_j^2)^2} \left(\frac{1}{N} \mathbf{y}_j - \omega_j \mathbf{C} \mathbf{x}_j \right), \quad \forall j = 1, \dots, C-1.$$

Proof. Recall $\mathbf{x}_j \in \mathbb{R}^{CN}$ is the j -th row of $\mathbf{X} \in \mathbb{R}^{C \times CN}$. Applying the flow definition in Equation 5 to the i -th element of \mathbf{x}_j gives

$$\begin{aligned}\frac{d}{dt} x_{ji} &= -\mathbf{e}_j^\top \Pi_{T_{\mathbf{X}} \mathcal{X}} \left(\frac{d\mathcal{L}_{\text{LS}}}{d\mathbf{X}} \right) \mathbf{e}_i \\ &= -\left\langle \Pi_{T_{\mathbf{X}} \mathcal{X}} \left(\frac{d\mathcal{L}_{\text{LS}}}{d\mathbf{X}} \right), \mathbf{e}_j \mathbf{e}_i^\top \right\rangle_F \\ &= -\left\langle \frac{d\mathcal{L}_{\text{LS}}}{d\mathbf{X}}, \Pi_{T_{\mathbf{X}} \mathcal{X}}(\mathbf{e}_j \mathbf{e}_i^\top) \right\rangle_F,\end{aligned}$$

where $\frac{d\mathcal{L}_{\text{LS}}}{d\mathbf{X}} \in \mathbb{R}^{C \times CN}$ is the standard derivative within the ambient $\mathbb{R}^{C \times CN}$ -space, $\mathbf{e}_i \in \mathbb{R}^{CN}$ and $\mathbf{e}_j \in \mathbb{R}^C$ are the canonical basis vectors, and $\langle \cdot, \cdot \rangle_F$ is the Frobenius matrix inner-product. Next, observe that the differential 1-form $d\mathcal{L}_{\text{LS}}(\cdot) : T_{\mathbf{X}} \mathcal{X} \rightarrow \mathbb{R}$ satisfies the following:

$$d\mathcal{L}_{\text{LS}}(\mathbf{Z}) = \left\langle \frac{d\mathcal{L}_{\text{LS}}}{d\mathbf{X}}, \mathbf{Z} \right\rangle_F, \quad \forall \mathbf{Z} \in T_{\mathbf{X}} \mathcal{X}.$$

Taking $\mathbf{Z} = \Pi_{T_{\mathbf{X}} \mathcal{X}}(\mathbf{e}_j \mathbf{e}_i^\top)$ then leads to

$$\begin{aligned}\frac{d}{dt} x_{ji} &= -d\mathcal{L}_{\text{LS}}(\Pi_{T_{\mathbf{X}} \mathcal{X}}(\mathbf{e}_j \mathbf{e}_i^\top)) \\ &= -\sum_{k=1}^{C-1} \frac{d\mathcal{L}_{\text{LS}}}{d\omega_k} d\omega_k (\Pi_{T_{\mathbf{X}} \mathcal{X}}(\mathbf{e}_j \mathbf{e}_i^\top)) \\ &= -\frac{d\mathcal{L}_{\text{LS}}}{d\omega_j} d\omega_j (\Pi_{T_{\mathbf{X}} \mathcal{X}}(\mathbf{e}_j \mathbf{e}_i^\top))\end{aligned}$$

where the second step follows by the chain rule, and the last step follows from Lemma 3 in that $d\omega_k (\Pi_{T_{\mathbf{X}} \mathcal{X}}(\mathbf{e}_j \mathbf{e}_i^\top)) = 0$ if $k \neq j$. Moreover, Lemma 3 also gives

$$d\omega_j (\Pi_{T_{\mathbf{X}} \mathcal{X}}(\mathbf{e}_j \mathbf{e}_i^\top)) = \left(\frac{1}{N} \mathbf{y}_j^\top - \omega_j \mathbf{x}_j^\top \mathbf{C} \right) \mathbf{e}_i.$$

It then follows that

$$\begin{aligned}\frac{d}{dt} \mathbf{x}_j &= -\frac{d\mathcal{L}_{\text{LS}}}{d\omega_j} \left(\frac{1}{N} \mathbf{y}_j - \omega_j \mathbf{C} \mathbf{x}_j \right) \\ &= \frac{\omega_j}{(C + \omega_j^2)^2} \left(\frac{1}{N} \mathbf{y}_j - \omega_j \mathbf{C} \mathbf{x}_j \right),\end{aligned}$$

where the last step follows from differentiating the expression in Lemma 1. \square

The gradient flows of \mathbf{x}_j induce the dynamics of ω_j , which are described below.

Lemma 5 (Induced Dynamics on SVD of SNR). *Under continually renormalized gradient flow (Equation 5), the dynamics for the j -th non-zero SNR singular value (Definition 2) is*

$$\frac{d}{dt}\omega_j = \frac{1}{N} \frac{\omega_j}{(C + \omega_j^2)^2}, \quad \forall j = 1, \dots, C-1. \quad (28)$$

Proof. Observation 1, the differential of the singular value decomposition (see Equation 17 of Townsend (2016)), and Observation 3 collectively imply that for any¹⁷ $d\mathbf{X} \in T_{\mathbf{X}}\mathcal{X}$,

$$d\omega_j(d\mathbf{X}) = \mathbf{e}_j^\top d\Omega(d\mathbf{X}) \mathbf{e}_j = \frac{1}{N} \mathbf{e}_j^\top d\mathbf{X} \mathbf{Y}^\top \mathbf{e}_j = \frac{1}{N} \mathbf{y}_j^\top d\mathbf{x}_j. \quad (29)$$

Recall that the differential of ω_j only depends on the differential of \mathbf{x}_j (see Lemma 3). Then, we can apply the chain rule:

$$\frac{d}{dt}\omega_j = \frac{d\omega_j}{d\mathbf{x}_j} \frac{d\mathbf{x}_j}{dt} = \frac{1}{N} \frac{\omega_j}{(C + \omega_j^2)^2} \mathbf{y}_j^\top \left(\frac{1}{N} \mathbf{y}_j - \omega_j \mathbf{C} \mathbf{x}_j \right), \quad (30)$$

where the last equality results substituting-in Lemma 4 and Equation 29. Since $\mathbf{Y}\mathbf{Y}^\top = N\mathbf{I}$,

$$\frac{1}{N^2} \mathbf{y}_j^\top \mathbf{y}_j = \frac{1}{N}.$$

Applying the same relation and Equation 22:

$$\mathbf{x}_j^\top \mathbf{C} \mathbf{y}_j = \mathbf{e}_j^\top \mathbf{X} \mathbf{C} \mathbf{Y}^\top \mathbf{e}_j = \frac{1}{CN} \mathbf{e}_j^\top \mathbf{X} \left(\mathbf{I} - \frac{1}{N} \mathbf{Y}^\top \mathbf{Y} \right) \mathbf{Y}^\top \mathbf{e}_j = 0.$$

Combining all the above equations, we obtain

$$\frac{d}{dt}\omega_j = \frac{1}{N} \frac{\omega_j}{(C + \omega_j^2)^2}.$$

□

The closed-form given in Proposition 2 now directly follows.

Proposition 2 (Dynamics of Singular Values of SNR Matrix). *Continually renormalized gradient flow on the central path (Equation 5) induces the following closed-form dynamics on the SNR singular values (Definition 2):*

$$c_1 \log(\omega_j(t)) + c_2 \omega_j^2(t) + c_3 \omega_j^4(t) = a_j + t, \quad t \geq 0, \quad \text{for all } j = 1, \dots, C-1. \quad (10)$$

c_1 , c_2 , and c_3 are positive constants independent of j , and a_j is a constant depending on $\omega_j(0)$.

Proof. Follows from symbolically solving the ODE in Lemma 5 with routine methods. The constants are $c_1 = C^2 N$, $c_2 = CN$, and $c_3 = \frac{N}{4}$. □

D.5 PROOF OF COROLLARY 1

Corollary 1 (Properties of SNR Singular Values). *SNR singular values (Definition 2) following the Equation 10 dynamics satisfy the following limiting behaviors:*

1. $\lim_{t \rightarrow \infty} \omega_j(t) = \infty$, for all $j = 1, \dots, C-1$.
2. $\lim_{t \rightarrow \infty} \frac{\omega_j(t)}{\sqrt{\frac{t}{c_4}}} = 1$, for all $j = 1, \dots, C-1$.
3. $\lim_{t \rightarrow \infty} \frac{\max_j \omega_j(t)}{\min_j \omega_j(t)} = 1$.

¹⁷For our goal of applying the chain rule in Equation 30, we can restrict our attention to just $d\mathbf{X} \in T_{\mathbf{X}}\mathcal{X}$: The definition of renormalized gradient flow (Equation 5) ensures that $\frac{d\mathbf{X}}{dt}$ will always be in $T_{\mathbf{X}}\mathcal{X}$.

Proof. As t tends to infinity, the right-hand side of Equation 10 diverges to infinity and therefore so does the left-hand side (LHS). As the LHS approaches infinity, the logarithmic terms become negligible compared to the dominant quartic term, implying $\omega_j^4(t) \rightarrow \infty$. Since $\omega_j(t)$ are singular values, they must be non-negative—implying $\omega_j(t) \rightarrow \infty$. Based on the same argument, observe that $\lim_{t \rightarrow \infty} \frac{\omega_j(t)}{\sqrt[4]{\frac{t}{c_3}}} = 1$ for all j . Since the constant c_3 is independent of j , it follows that $\lim_{t \rightarrow \infty} \frac{\max_j \omega_j(t)}{\min_j \omega_j(t)} = 1$. \square

D.6 PROOF OF COROLLARY 2

Corollary 2 (Neural Collapse under MSE Loss). *The SNR matrix (Equation 9) converges to*

$$\lim_{t \rightarrow \infty} \frac{1}{\omega_{\max}(t)} \text{SNR}_t = \hat{\mathbf{U}}_0 \hat{\mathbf{V}}_0^\top, \quad (11)$$

where $\hat{\mathbf{U}}_0 \in \mathbb{R}^{P \times (C-1)}$ and $\hat{\mathbf{V}}_0 \in \mathbb{R}^{C \times (C-1)}$ are the left and right singular vectors of the SNR matrix (Definition 2) at $t=0$ corresponding to the non-zero singular values; and $\omega_{\max}(t)$ is the largest singular value at time t . Corollary 1 and Equation 11 together imply the occurrence of (NC1)-(NC4) i.e. renormalized gradient flow on the central path leads to Neural Collapse.

Moreover, denoting the Kronecker product with \otimes , the renormalized features matrix converges to

$$\lim_{t \rightarrow \infty} \frac{1}{\omega_{\max}(t)} \Sigma_{W,t}^{-\frac{1}{2}} \bar{\mathbf{H}}_t = (\hat{\mathbf{U}}_0 \hat{\mathbf{V}}_0^\top) \otimes \mathbf{1}_N^\top. \quad (12)$$

Proof. Consider the normalized SNR matrix $\frac{1}{\omega_{\max}(t)} \text{SNR}_t$ at time t . Corollary 1 proves the singular values $j = 1, \dots, C-1$ of SNR_t diverge to infinity and that their ratio tends to one. (The C -th singular value is 0 due to the zero global-mean.) Hence, (every convergent subsequence of) $\frac{1}{\omega_{\max}(t)} \text{SNR}_t$ converges to a Simplex ETF. This gives (NC2).

Lemma 1 shows that the MSE loss on the central path depends only on the singular values, and not on the singular vectors, of the matrices SNR_t and Ω_t . As a result, the gradient of $\mathcal{L}(\omega(t))$ does not depend on the singular vectors of these matrices. Thus, the renormalized gradient flow will not change the singular vectors of these matrices, and we get the limit in Equation 11.

Based on Equation 11, we deduce the within-class covariance, $\Sigma_W \left(\frac{1}{\omega_{\max}(t)} \mathbf{X}_t \right)$, becomes negligible compared to the between-class covariance. Therefore, the normalized matrix $\frac{1}{\omega_{\max}(t)} \mathbf{X}_t$ undergoes activation collapse (NC1). From Theorem 1 of Pappas, Han, and Donoho (2020), we then know that (NC3) and (NC4) follow from (NC1) and (NC2) on the central path.

Combining the limit in Equation 11 with (NC1) proves the limit in Equation 12. \square

E RELATED WORKS EXAMINING NEURAL COLLAPSE

In this section, we discuss the contributions and limitations of seven recent works that propose and analyze theoretical abstractions of Neural Collapse. These works are only available in preprint, and may not yet be peer-reviewed. Thus, they might ultimately appear with very different claims or results. Additionally, works such as Poggio & Liao (2020a;b); Ergen & Pilanci (2020) also analyze behaviors other than NC; we will only discuss the parts relevant to Neural Collapse here.

E.1 MIXON, PARSHALL, AND PI (2020)

Mixon et al. (2020) considered the unconstrained features model in Equation 2 (without weight decay) where, under gradient flow, (\mathbf{W}, \mathbf{H}) evolve according to a nonlinear ordinary differential equation (ODE). They followed a two-step strategy for studying Neural Collapse. First, they linearized the ODE—claiming nonlinear terms are negligible for models initialized near the origin—and proved the simplified ODE converges to a subspace of (\mathbf{W}, \mathbf{H}) satisfying (NC1) and (NC3). Second, they proved that gradient flow, restricted to that subspace, converges to (NC2).

The assumption of small weights and classifiers leading to the linearized ODE is not aligned with today’s paradigm. Specifically, the most commonly used He initialization (He et al., 2015) is designed: (i) to create weights with non-negligible magnitude; and (ii) to preserve the magnitude of features, as they propagate throughout the layers of the network, exactly so that last-layer features would have non-negligible magnitude. Moreover, the analysis of Mixon et al. essentially assumes that (NC1) and (NC3) occur much sooner than (NC2). However, from the experiments in both Pappan, Han, and Donoho (2020) and this paper, there is no empirical evidence that (NC2) happens slower than (NC1) and (NC3) in practice.

E.2 LU AND STEINERBERGER (2020)

While the MSE loss provides a mathematically natural setting for analysis, the modern paradigm in multi-class classification with deep learning involves training with CE loss, which is more challenging to analyze than MSE.

Lu & Steinerberger (2020) studied the (one-example-per-class) unconstrained¹⁸ features model with CE loss:

$$\min_{\mathbf{W}, \mathbf{M}} \text{CE}(\mathbf{W}, \mathbf{M}) \quad \text{s.t.} \quad \|\mathbf{w}_c\|_2 = \|\boldsymbol{\mu}_c\|_2 = 1.$$

Since under linear separability the CE loss can be driven arbitrarily close to zero, just by re-scaling the norms of \mathbf{W} and \mathbf{M} , the authors further imposed a norm constraint on \mathbf{w}_c and $\boldsymbol{\mu}_c$. Lu & Steinerberger observe that the global minimizer of this optimization problem is only achieved once \mathbf{W} and \mathbf{M} are the same Simplex ETF. This derivation is suggestive, but it does not identify closed-form dynamics which would get gradient flow to such a global minimizer, nor does it address the rate of convergence to Neural Collapse. Additionally, the constraint on $\boldsymbol{\mu}_c$ possesses no immediate or direct analogy to standard deep net training—where procedures often control the norm of the weights \mathbf{W} , but not features \mathbf{H} —nor class-means \mathbf{M} .

E.3 E AND WOJTOWYTSCH (2020)

E & Wojtowytsch (2020) also consider the unconstrained features model¹⁸ with CE loss,

$$\min_{\mathbf{W}, \mathbf{H}} \text{CrossEntropy}(\mathbf{W}\mathbf{H}) \quad \text{s.t.} \quad \|\mathbf{W}\|_2 \leq 1, \|\mathbf{h}_{i,c}\|_2 \leq 1,$$

where they adopt a more technical, *spectral* norm constraint on \mathbf{W} to specify their model.

Building on the results of Chizat & Bach (2018; 2020), E & Wojtowytsch also construct a simple counter-example showing that Neural Collapse need not occur in two-layer, infinite-width networks—which have been the focus of intense recent study in the theoretical deep learning community (Mei et al., 2018; Rotskoff & Vanden-Eijnden, 2018; Arora et al., 2019). Thus, E & Wojtowytsch’s counterexample suggests the alternative perspective that, despite the expressiveness of infinite-width, two-layer networks, such abstractions do not capture key aspects of trained *deep* nets.

As with Lu & Steinerberger (2020), standard deep net training does not possess any direct analogies for constraining the norm of *features* (as opposed to weights)—nor are there any paradigmatic regularizations that correspond to controlling the *spectral* norm on \mathbf{W} . Moreover, the work does not characterize any closed-form dynamics or the rate of convergence to Neural Collapse.

E.4 POGGIO & LIAO (2020A;B) (WITH BANBURSKI)

Distinguished from the simplified unconstrained features models in the previously mentioned works is the theoretical analysis of Poggio & Liao (2020a;b) (in a special section, co-authored with Andrzej Banburski).

The authors study deep homogeneous classification networks, with weight normalization layers, trained with stochastic gradient descent and weight decay. This is much closer to today’s training paradigm, but the setting still differs from the one in which Neural Collapse has been empirically

¹⁸The model is unconstrained in the sense that the features are allowed to move directly with gradient flow and are not constrained to be the output of a forward pass—not in the sense that there are no constraints on the optimization problem.

observed in Pappan, Han, and Donoho (2020) and in Section A of this paper. In particular, they replace batch normalization with weight normalization and consider deep homogeneous networks; homogeneous networks can not have bias vectors nor skip connections, which are present both in ResNet and DenseNet. Moreover, the work gives explicit descriptions of neither the dynamics nor the rate of convergence to Neural Collapse.

E.5 ERGEN & PILANCI (2020)

While the above-described works tend to focus on either the used-in-practice CE loss or the theoretically-insightful MSE loss, Ergen & Pilanci (2020) observed that these are both instances of the general class of convex loss functions and, thus, one could derive insights from the classical convex analysis literature. Moreover, compared to Mixon et al. (2020); Lu & Steinerberger (2020); E & Wojtowysch (2020), this work studies the optimization starting from the *second*-to-last layer features rather than the last-layer features. In particular, the authors use a strong-duality argument to show that NC emerges in the optimal solution of an equivalent proxy-model to the following optimization:

$$\min_{\mathbf{H}_{L-1}, \mathbf{W}_{L-1}, \mathbf{W}_L, \gamma, \alpha} \mathcal{L} \left(\mathbf{W}_L (\text{BN}_{\gamma, \alpha} (\mathbf{W}_{L-1} \mathbf{H}_{L-1}))_+, \mathbf{Y} \right) + \frac{\lambda}{2} \left(\|\gamma\|_2^2 + \|\alpha\|_2^2 + \|\mathbf{W}_L\|_F^2 \right),$$

where $\mathcal{L}(\cdot)$ is a general convex loss, \mathbf{H}_{L-1} are the second-to-last layer activations, \mathbf{W}_{L-1} are the second-to-last layer weights, \mathbf{W}_L are the network classifiers, \mathbf{Y} are the training targets, λ is a weight-decay parameter, $\text{BN}_{\gamma, \alpha}(\cdot)$ is a batch-norm operator parameterized by α and γ , and $(\cdot)_+$ is a ReLU. The incorporation of batch-normalization and weight-decay ensures the existence of bounded, well-defined optimal solutions—serving a similar role to that of weight-normalization and weight decay in Poggio & Liao (2020a;b) as well as the norm constraints in the other aforementioned related works.

Since strong-duality only characterizes properties of the converged optimal solution of an optimization model, Ergen & Pilanci (2020) does not provide insights into the dynamics with which that solution is achieved which training.

E.6 FANG, HE, LONG, AND SU (2021)

In Fang et al. (2021), the authors introduce the (*N*-)layer-peeled model in which one considers only the direct optimization of the *N*-th-to-last layer features of a deep net along with the weights that come after the *N*-th-to-last layer. The motivating philosophy is that, after raw inputs are passed through some initial number of layers, the overparameterization of those layers would allow us to effectively model the *N*-th-to-last layer features as freely-moving in some subset of Euclidean space. In this terminology, the concurrent works of Mixon et al. (2020); Lu & Steinerberger (2020); E & Wojtowysch (2020) on the unconstrained (last-layer) features model could be considered instances of a 1-layer-peeled model; while the model of Ergen & Pilanci (2020) could be considered as a 2-layer-peeled model. This perspective is attractive because it gives a name and organization to a common modeling philosophy behind the above-described body of independent works. For comparison, the work of Poggio & Liao (2020a;b) is a non-example of layer-peeled modeling as it considers optimization on the weights of homogeneous deep nets and not the input features.

Fang et al. (2021) then analyzes a convex relaxation of the 1-layer-peeled model—with norm constraints on the weights and features—into a semidefinite program. Not only do the authors show that this model exhibits Neural Collapse in the canonical setting of balanced examples-per-class, but they also analyze the behavior of this model under *imbalanced classes*. While, in the imbalanced case, one would intuitively expect the Simplex ETF to “skew” to have bigger angles around over-represented classes and smaller angles around under-represented ones; Fang et al. (2021) identifies the surprising phenomenon—named *minority collapse*—in their model where, when the imbalances pass a certain threshold, *the last-layer features and classifiers of the under-represented classes collapse to be exactly the same*. However, their work does not provide closed-form dynamics or rates at which collapse—in either the balanced or imbalance case—occurs.

E.7 ZHU, DING, ZHOU, LI, YOU, SULAM, AND QU (2021)

In Zhu et al. (2021), the authors examine the following unconstrained features model:

$$\min_{\mathbf{W}, \mathbf{H}, \mathbf{b}} \text{CrossEntropy}(\mathbf{W}\mathbf{H} + \mathbf{b}, \mathbf{Y}) + \frac{\lambda_{\mathbf{W}}}{2} \|\mathbf{W}\|_F^2 + \frac{\lambda_{\mathbf{H}}}{2} \|\mathbf{H}\|_F^2 + \frac{\lambda_{\mathbf{b}}}{2} \|\mathbf{b}\|_F^2,$$

where (\mathbf{W}, \mathbf{b}) are the classifier weights and biases, \mathbf{H} are the last layer features, and $(\lambda_{\mathbf{W}}, \lambda_{\mathbf{H}}, \lambda_{\mathbf{b}})$ are weight-decay parameters. On this model, the authors not only prove that all minima exhibit Neural Collapse but also that *all local minima are global minima*. In comparison to our current paper, Zhu et al. (2021) focus on characterizing the landscape of the loss and, thus, do not explore the dynamics and rate at which such minimizers of the loss are achieved.

Zhu et al. (2021) also make notable empirical contributions by conducting a series of experiments on the MNIST and CIFAR10 datasets trained on MLPs, ResNet18, and ResNet50. Their measurements give evidence for the following novel NC-related phenomena in deep classification networks:

1. **NC is algorithm independent:** NC emerges in realistic classification deep net training regardless of whether the algorithm is SGD, ADAM, or L-BFGS.
2. **NC occurs on random labels:** NC emerges even when the one-hot target vectors are completely shuffled.
3. **Width improves NC:** Increasing network width expedites NC when training with random labels.

The authors of Zhu et al. (2021) moreover conducted ablation experiments suggesting that the following substitutions can be made to deep neural net architectures without affecting performance:

1. **Weight-decay substitution:** Replacing (A) weight-decay on the norm of all network parameters with (B) weight-decay just on the norm of the last-layer features and classifiers.
2. **Classifier substitution:** Replacing (A) the last-layer classifiers that are trained with SGD with (B) Simplex ETF classifiers that are fixed throughout training.

While the authors only demonstrated these new behaviors on limited network-dataset combinations, these experiments indeed inspire interesting conjectures about the generalization behavior of deep nets as well as potential architecture design improvements; Zhu et al. (2021) discuss many of these conjectures and related open-questions in detail.